Parametric Roll Resonance Monitoring using Signal-based Detection

Roberto Galeazzi[a,*], Mogens Blanke[a,b], Thomas Falkenberg[a], Niels K. Poulsen[c], Nikos Violaris[d], Gaute Storhaug[d], Mikael Huss[e]

[a]*Department of Electrical Engineering, Technical University of Denmark, DK 2800, Kongens Lyngby, Denmark*
[b]*AMOS Centre of Excellence, Institute for Technical Cybernetics, Norwegian University of Science and Technology, NO 7491, Trondheim, Norway*
[c]*Department of Applied Mathematics and Computer Science, Technical University of Denmark, DK 2800, Kongens Lyngby, Denmark*
[d]*DNV-GL, NO 1322, Høvik, Norway*
[e]*Wallenius Marine, SE 17086, Stockholm, Sweden*

Abstract

Extreme roll motion of ships can be caused by several phenomena, one of which is parametric roll resonance. Several incidents occurred unexpectedly around the millennium and caused vast fiscal losses on large container vessels. The phenomenon is now well understood and some consider parametric roll a curiosity, others have concerns. This study employs novel signal-based detection algorithms to analyse logged motion data from a container vessel (2800 TEU) and a large car and truck carrier (LCTC) during one year at sea. The scope of the study is to assess the performance and robustness of the detection algorithms in real conditions, and to evaluate the frequency of parametric roll events on the selected vessels. Detection performance is scrutinised through the validation of the detected events using owners' standard methods, and supported by available wave radar data. Further, a bivariate statistical analysis of the outcome of the signal-based detectors is performed to assess the real life false alarm probability. It is shown that detection robustness and very low false warning rates are obtained. The study concludes that small parametric roll events are occurring, and that the proposed signal-based monitoring system is a simple and effective mean to provide timely warning of resonance conditions.

Keywords: Parametric roll resonance, Statistical change detection, Ship stability, Full-scale validation

1. Introduction

Parametric roll resonance in head seas is one of the phenomena that can create extreme roll motion of ships. This type of roll motion can grow exponentially to extreme values that

*Corresponding author at: DTU Electrical Engineering, Technical University of Denmark, DK 2800, Kongens Lyngby, Denmark.
Tel.: +45 45253549; Fax: +45 45881295
Email addresses: rg@elektro.dtu.dk (Roberto Galeazzi), mb@elektro.dtu.dk (Mogens Blanke), nkpo@dtu.dk (Niels K. Poulsen), Nikos.Violaris@dnvgl.com (Nikos Violaris), Gaute.Storhaug@dnvgl.com (Gaute Storhaug), Mikael.Huss@walleniusmarine.com (Mikael Huss)

Article accepted for publication by Ocean Engineering *October 2, 2015*

cause considerable damage to cargo and also include the risk of capsizing. The phenomenon created international awareness when roll resonance events occurred on large container vessels and caused huge fiscal losses before and after the Millennium. Training of navigators has helped to improve ship's ability to escape from most of the severe consequences if getting subjected to parametric roll resonance, but events on both container vessels and car carriers indicate that the phenomenon persists. Following stringent methods to characterize parametric resonance, this paper exploits a signal based approach to analyse and detect parametric roll.

Significant research followed the APL China event in 1998 (France et al., 2001) and that on Maersk Carolina in 2003 (Carmel, 2006). The hydrodynamic effects that cause parametric roll resonance are now well understood to be phenomena described by the behaviour of nonlinear differential equations with time-varying parameters, (Hashimoto and Umeda, 2004), (Bulian et al., 2008), and complex mathematical models have been published to simulate roll resonance behaviour (Neves and Rodriguez, 2005, 2006), (Holden et al., 2007a). The likelihood of getting into a parametric roll resonance condition was investigated using first order reliability analysis methods by Jensen (2007, 2012) showing a low but non negligible likelihood of large resonance events. An overview of the phenomenon and its characteristics was presented in (Døhlie, 2006). Despite the awareness, events do occur and three cases were recently reported from car carriers (Rosén et al., 2012). The analysis of roll resonance events has so far been mainly a manual effort but novel results on signal based automated detection (Galeazzi et al., 2013) suggested a methodology to detect resonance events from low-cost motion sensor information. However, this method was not evaluated on long-term voyage data and not on full-scale resonance events, due to lack of real life data.

This paper fills this gap of knowledge by analysing long-term data for two different vessels: selected parts of data from a 2800 TEU container vessel for which data were available over a 2 year period, and motion data from all voyages of a large car carrier over a one year period. Furthermore, motion data from two of the parametric resonance events reported in the literature have been made available for this study. The paper employs the signal-based, stochastic change detection method (Galeazzi et al., 2012b)[1], (Galeazzi et al., 2013) that will alert when motion signals indicate that a vessel is close to or already in roll resonance. The monitoring system employs two detectors: one evaluates whether pitch and roll are close to a 2:1 ratio in frequency, the other tests the phase alignment between pitch and roll. A resonance event is diagnosed when both indicators are positive. Wave radar data are used as an independent source of information to characterise sea conditions.

The paper presents long-term results for the ships mentioned and demonstrates how timely detection is achieved using only motion signals from inexpensive inertial measurement units onboard. Detection performance is scrutinised and statistics of maximum roll amplitudes, time from detection to maximum roll, etc, are presented. The events detected by the monitoring system are validated by DNV-GL and Wallenius Marine according to the manual evaluation criteria they use. A scrutiny is then made of the bivariate distribution of data from the combined detectors to assess the false alarm probability, and analysis of the joint distributions shows that a very low false alarm probability can be achieved. The paper documents that parametric roll resonance is still a risk, despite increased awareness of the phenomenon, and that signal-based detection is a simple and effective method to provide early warning.

[1]The detection methods are patented under EP2419804 by the Technical University of Denmark and are available on royalty terms

The paper is organized as follows: Section 2 explains parametric resonance as one of the phenomena that cause large and rapidly growing roll motion and explains the seamanship required to escape from a parametric roll condition if the resonance has been triggered; Section 3 presents a mathematical treatment of parametric roll resonance and gives the empirical conditions for its onset; Section 4 introduces the full-scale motion data and analyses the presence of resonance phenomena on two vessels based on time and frequency domain analysis; Section 5 introduces signal-based detection methods, it discusses the selection of thresholds and shows how robustness can be achieved through combined hypothesis testing; Section 6 discusses the findings from applying the condition monitoring on two years of fast sampled motion data from the two vessels; Section 7 explains how ship operators are managing the risk associated with parametric roll; Section 8 offers conclusions and addresses topics of further research.

2. Large Roll Motion in Context

A ship's life consist of a design phase, the operation, and the end-of-life scrapping. The design and scrapping phases are relatively short while operation is in the order of 25 years. It is therefore not only important to design the vessel for its intended operation, but also to safeguard the vessel, crew and cargo during its operation. During design, there are functional requirements that should be satisfied. A design need to be made according to classification society rules, which include regulations by IMO (International Maritime Organisation) and others. These rules may not cover all aspects and they are based on assumptions to the design. The assumptions may be related to the amount of cargo allowed on board and also the roll angles and accelerations, which are used in the design calculations to simultaneously secure the cargo and to ensure that the hull is not damaged by the cargo. It is implicit that these assumptions are not being exceeded during the operation.

Excessive roll angles can clearly cause damage, and the physical reasons for large roll motion in waves can have several reasons (France et al. (2001), Boonstra et al. (2006), Bulian et al. (2008), Rosén et al. (2012), Krüger et al. (2013)): parametric roll, of which the 2:1 resonance is most common; forced roll in stern quartering or beam seas; resonance roll motions in stern or beam seas; broaching caused by loss of directional stability when relative water particle velocity at the rudder is low; loss of stability due to loss of water line area in front and aft when stuck on a wave crest; loss of stability due to maneuvering and water on deck and lost remaining stability.

Some of these phenomena are well understood and known by the officers on board, others are less well known and further development of decision support systems and training are needed. Based on reports of vessels exceeding 30 degrees roll, in the references above, IMOs Maritime Safety Committee issued a circular describing events of extreme roll and emphasized parametric resonance as one of the phenomena giving rise to unexpected and rapidly growing roll motion.

During operation the seamanship is important. The Master should ensure that the vessel is not overloaded and that the roll angles and accelerations do not exceed acceptable levels. This may be difficult to ensure, but the navigators have various tools at hand to provide decision support. Examples are systems that provide weather information, calculate the loading conditions and monitor hull stress. Nevertheless, a large number of containers falls over board or is getting damaged each year. The international joint industry project *Lashing@Sea* (Koning, 2010) estimates this number to be 10000 per year and states that it is not an insignificant number of vessels that are involved annually. Decision support systems were developed following the APL China incident. A framework of an Active Operator Guidance system was made by DNV, and industrial vendors have made commercially available decision support systems for this purpose.

It could be questioned why large roll incidents still happen and weather the decision support systems at hand are sufficient. One answer is that excessive roll can have several causes and another that parametric resonance has apparently not been detected with sufficient accuracy in present systems.

This paper presents extensive testing and refinement of the parametric roll detection method (PAROLL) the theory of which was described in (Galeazzi et al., 2012a, 2013). Some of the data include several events that were reported as parametric resonance while the majority of records show only forced roll. The presence of both conditions gives a unique opportunity to investigate both detection performance and false alarm probabilities. Three features have been added to the condition monitoring system to enhance its operational usability. A colour coded risk coefficient informs about how close the vessel is to experience a parametric roll event. An audible alarm is only issued after further real-time checks on a) exponential growth of the roll and b) a check on the magnitude of roll angle. With these additional indicators to filter an already very low false alarm rate, exceptional performance is shown to be obtained in false alert properties of the algorithms, yet leaving detection agile and timely to make navigators able to react with remedial actions if in risk.

2.1. Escaping from resonance conditions

Courses are given worldwide to create awareness on parametric roll, and on how to escape a resonance condition. The parametric roll detection system presented in this paper may contribute to build awareness on board. While the existing decision support systems suggest what is the critical sea state, the algorithms presented in this paper also detect the risk of synchronization, which is needed to develop parametric roll, and the system can warn about this early in the build-up.

This makes it possible both to change the conditions by altering course and varying forward speed to move away from the critical sea state, but also to prevent parametric roll to develop to high roll angles during build up. One should prevent that roll angles on car carriers exceed 10-12 degrees, slightly higher values can be tolerated on container vessels. Early detection of parametric roll may be useful also for other ship types with pronounced bow flare and over hanging stern, including fishing vessels, ro-ro vessels and cruise vessels.

The immediate means to de-tune a resonance is to change the encounter frequency of the waves. This is done by altering the heading and/or changing the ship's speed. De-tuning of a parametric roll condition can be done within 30-60 seconds, i.e 1.5 to 3 roll cycles, under alert conditions. Detection is considered early if an alert is timely enough to allow remedial action to take place before roll angles have reached the critical levels.

3. Mathematical Preliminaries on Parametric Roll Resonance

To establish a background for understanding the detection principles used in this paper, we first give a brief account of the mathematics behind parametric roll resonance. While more complex models are available Neves and Rodriguez (2006) and references herein, a two degrees-of-freedom non-dimensional model in pitch θ and roll ϕ suffice to describe the resonance phenomenon Tondl et al. (2000), and a useful conceptual model is,

$$\ddot{\theta} + \upsilon_\theta \dot{\theta} + \omega_\theta^2 \theta + \kappa_\theta(\theta, \phi, t) = \zeta \cos\left(\omega_e t + \xi_\zeta\right) \tag{1}$$

$$\ddot{\phi} + \upsilon_\phi(\dot{\phi})\dot{\phi} + \omega_\phi^2 \phi + \kappa_\phi(\theta, \phi, t) = 0 \tag{2}$$

where υ_θ is the linear damping in pitch; $\upsilon_\phi(\dot{\phi}) \triangleq \upsilon_{\phi,l} + \upsilon_{\phi,n}(\dot{\phi})$ is the linear ($\upsilon_{\phi,l}$) plus nonlinear ($\upsilon_{\phi,n}$) damping in roll; ω_θ is the pitch natural frequency; ω_ϕ is the roll natural frequency; $\kappa_\theta(\theta, \phi, t)$ and $\kappa_\phi(\theta, \phi, t)$ are nonlinear restoring moments in pitch and roll; ζ, ω_e, and ξ_ζ are the wave amplitude, wave encounter frequency, and phase shift respectively. A detailed description of the model (1)-(2) can be found in (Galeazzi et al., 2013).

The system (1)-(2) admits two types of solutions. Let ζ_c be the critical value of the external excitation that triggers parametric resonance, then a first order approximation to the solution of (1)-(2) reads,

- if $0 < \zeta < \zeta_c$ a bounded and stable solution exists

$$\theta(t; \epsilon) = A_\theta \cos(\omega_e t + \xi_\theta) + O(\epsilon) \quad t \geq 0 \tag{3}$$

$$\phi(t; \epsilon) = 0 \tag{4}$$

  that is there is no roll motion and the pitch motion has an amplitude growing linearly with ζ,

- if $\zeta > \zeta_c$ an unbounded and unstable solution appears in roll,

$$\theta(t; \epsilon) = A_\theta \cos(\omega_e t + \xi_\theta) + O(\epsilon) \quad t \geq 0 \tag{5}$$

$$\phi(t; \epsilon) = \alpha_\phi(\epsilon t) \cos\left(\frac{1}{2}\omega_e t - \xi_\phi(\epsilon t)\right) + O(\epsilon) \quad t \geq 0 \tag{6}$$

  where $\alpha_\phi(\epsilon t)$ is an exponential envelop that grows with time. The roll motion shows an unbounded oscillatory behaviour, with oscillations occurring at half the wave encounter frequency ω_e.

The amplitude and phase shift of pitch are,

$$A_\theta = \frac{\zeta}{\sqrt{(\omega_\theta^2 - \omega_e^2)^2 + \omega_e^2 \upsilon_\theta^2}}, \quad \xi_\theta = \arctan\left(-\frac{\omega_e \upsilon_\theta}{\omega_\theta^2 - \omega_e^2}\right).$$

Application of Floquet theory (Grimshaw, 1993) determines the boundaries of the principal instability region of (2) to be,

$$\frac{1}{4}\frac{\upsilon_{\phi,l}^2}{\omega_e^2} + \left(\frac{\omega_\phi^2}{\omega_e^2} - \frac{1}{4}\right)^2 = \frac{1}{4}\frac{\eta^2}{\omega_e^4}, \tag{7}$$

where $\eta \triangleq \eta(\zeta, \omega_\theta, \omega_e, \upsilon_\theta)$ is the amplitude of the parametric excitation. The boundary condition (7) can be used to determine the critical value ζ_c (see (Tondl et al., 2000, Chapter 4), (Galeazzi et al., 2013)).

When the amplitude of parametric excitation crosses the critical value, the amount of energy stored in the pitch mode stays constant and the entire energy rise flows into the roll mode. The rate at which energy is pumped into the roll motion varies according to the change of the phase ξ_ϕ. When the rate at which energy being dissipated by viscous effects has matched the rate at which energy is transferred to the roll subsystem, this system reaches a motion characterized by a constant amplitude and a phase shift $\xi_\phi = \pi$.

The empirical conditions that may trigger parametric roll resonance in the principal parametric resonance region are,

	DNV1	DNV2	DNV3	DNV4	WM1	WM2
Start [hh:mm]	17:30	00:00	03:30	19:00	21:00	02:00
Stop [hh:mm]	23:59	21:30	22:00	23:30	01:00	07:00
U_{av} [kn]	–	–	5–11	–	5–11	9–14
T_ϕ [s]	22	22	22	22	28	21
$\phi_{\max}$ [deg]	-19.81	23.24	21.35	-20.55	-27.94	19.15
$\theta_{\max}$ [deg]	-5.16	-9.06	-6.34	-4.49	-2.69	4.95
H_s [m]	5–6	4–7	4–8	5–6	4	5–6
T_p [s]	10–11	11–16	11–14	11	9.2	11–13.5
ψ_e [deg]	150–160	140–180	140–180	170	0	140–190

Table 1: DNV-GL and Wallenius Marine data sets with reported parametric resonance.

1. the period of the encounter wave is approximately equal to half the natural period of the roll ($T_e \approx 0.5T_\phi$),
2. the wavelength and ship length are approximately equal,
3. the wave height is larger than a ship-dependent threshold.

4. Parametric Roll Events

Among the reported events of parametric roll, data sets were made available for this study from two types of vessels. One set was made available by DNV-GL from a 2800 TEU container vessel, where in particular four days of navigation had been identified by DNV-GL to have parametric roll resonance events. Records were made available for close to one year of passage data for this vessel. These data are presented in Section 4.1. A second set of data, provided by Wallenius Marine, consists of navigational records from two different large car and truck carries (LCTC) where events had been reported (Rosén et al., 2012). These data are presented in Section 4.2. In addition to the data where parametric roll events were known to exist, a one-year set of data from yet another LCTC were made available in order to make a blind test of the monitoring algorithms. The results of the blind test are reported in Section 6.3.

4.1. DNV-GL data from 2800 TEU container vessel

The full scale data set provided by DNV-GL covers several months of voyage data from a 2800 TEU container vessel. Four days of navigation in the middle of the winter period have been extracted because manual analysis in (Døhlie, 2006) pointed to several cases of parametric roll. Therefore, these sequences of data provide unique possibility of validating the detection methods. Figure 1 illustrates the evolution of the sea state in terms of significant wave height H_s, wave peak period T_p, and wave encounter angle ψ_e during the four days when the parametric roll events were experienced. H_s and T_p are extracted from wave radar data. The coloured areas in the Figure highlight the time periods within which the ship's motions are analysed in this paper. Table 1 summarizes some information about the four data subsets named DNV1 to DNV4, where U_{av} is the average ship's forward speed; T_ϕ is the roll natural period; $\phi_{\max}$ and $\theta_{\max}$ are the largest roll and pitch angles.

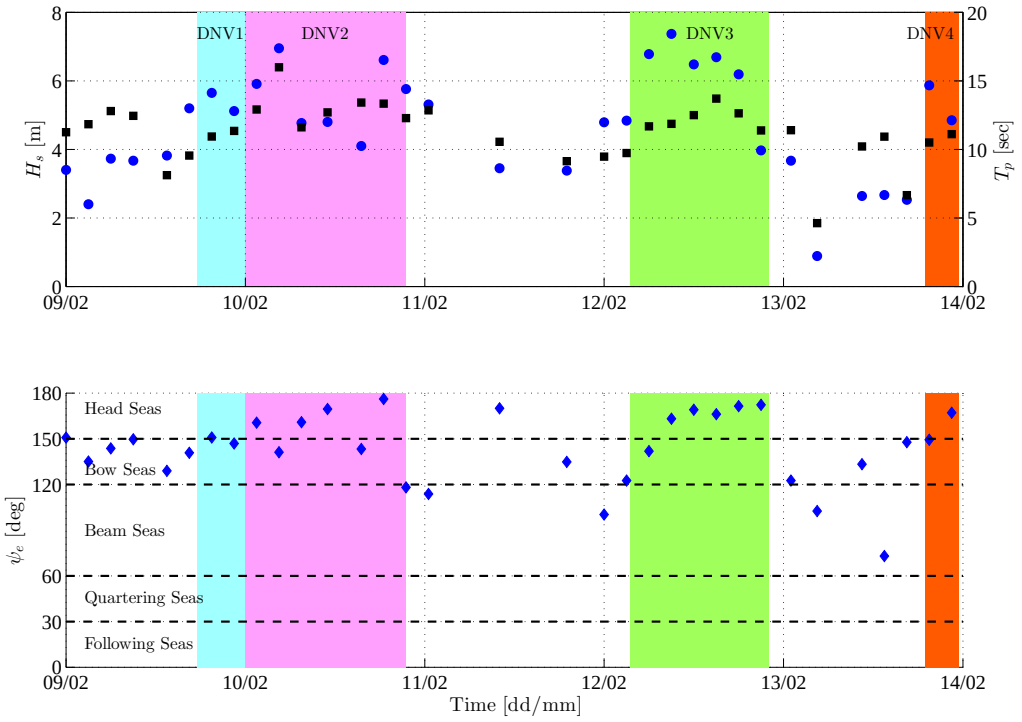

Figure 1: Sea state information for the DNV-GL data sets. In the top plot the evolution of the significant wave height H_s (blue cirlces) is shown together with the peak period T_p (black squares): the vessel was in moderate to heavy seas for several days.

With H_s 4-8 m (Beaufort 5-7) from ahead, and T_p close to $0.5T_\phi$ the vessel was exposed to conditions that could lead to the onset and development of parametric roll for most of time during the four days. This is observed from excerpts of the time series. Figure 2 shows the sailing conditions and motions (roll and pitch angles) during the first eight hours of the DNV3 record. Wave radar measured directional spectra at time 06:30 and 08:30 are also shown, where head seas correspond to 0 deg.

The container vessel navigates in 7-8 m seas; the wave encounter angle $\psi_{e,\text{av}}$ comes closer to 180°, and the forward speed U_{av} is reduced. This is considered a standard procedure applied by the Masters to protect the vessel and the cargo from large transversal accelerations.

This, however, in combination with the wave peak period ($T_p \approx 11$ s) gives a 2:1 ratio between the wave encounter frequency ω_e and the roll natural frequency ω_ϕ, as shown in the second topmost plot, and makes, for several hours, the vessel a potential subject for parametric roll.

Figure 3 shows a 3 hours excerpt of the data set DNV4, where the roll and pitch angles are shown together with the wave directional spectrum at time 20:00 and 21:30, and the normalized pitch and roll power spectral densities. The time and frequency domain integrated analysis of the relevant ship motions points to the conclusion that also this data set has clear cases of parametric roll resonance. This data exemplifies how essential the phase synchronization of pitch and roll is for the development of parametric roll. Although the frequency condition is fulfilled at least one

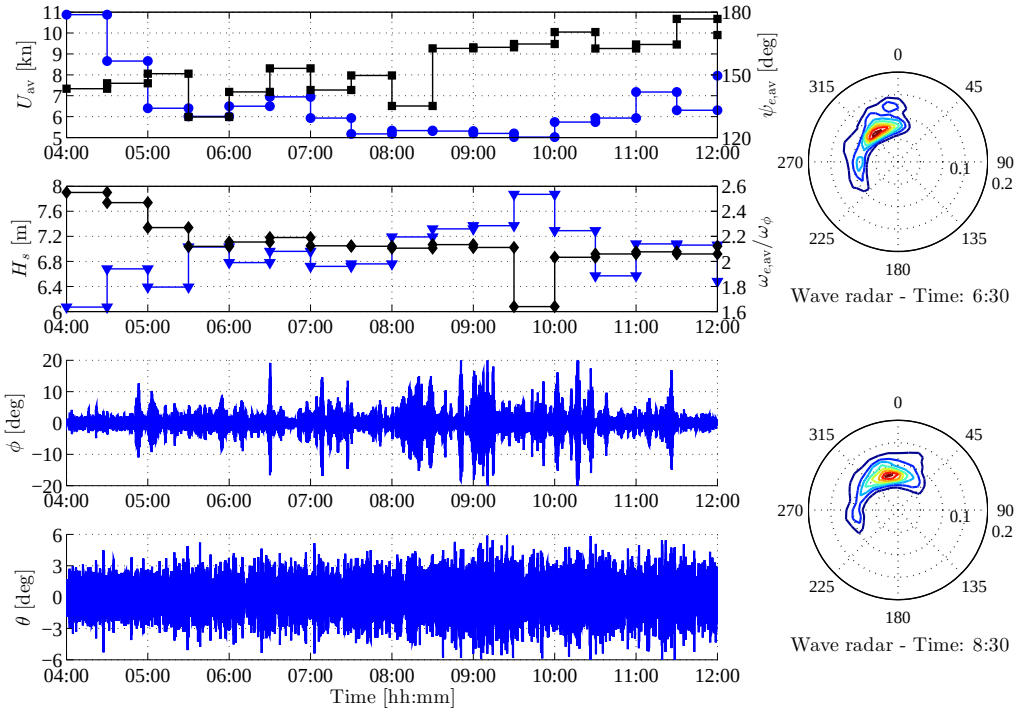

Figure 2: Excerpt of the data set DNV3 from 04:00 to 12:00 hours: the container ship navigates with H_s = 6-8 m (blue triangles); the forward speed U_{av} (blue dots) is gradually reduced and the waves' encounter angle ψ_{av} (black squares) becomes close to zero. This combination gives frequency ratio $\omega_{e,\text{av}}/\omega_\phi$ around 2 (black diamonds).

hour prior to the first resonant event, parametric roll does not develop until few minutes before 21:00 when waves cause a synchronous motion between pitch and roll. This is shown in the bottom left corner plot.

4.2. Wallenius Marine data from LCTC vessels with reported events

The full scale data set provided by Wallenius Marine consists of two occurrences of parametric roll resonance on board LCTC vessels (Rosén et al., 2012). Table 1 gives some information about the two data subsets named WM1 and WM2.

The first set (WM1) shows a 2:1 principal parametric resonance event in following seas. Forward speed, heading, roll and pitch angles are shown in Fig. 4. The vessel waited for few hours in head sea ($\psi \approx 180°$) at low speed ($U \approx 5$ kn) outside a harbour closed due to heavy weather. Roll and pitch oscillations were well below 5 degrees. Approximately 20 minutes after the vessel finished a turning manoeuvre, an unforeseen large roll motion developed quickly with roll amplitude reaching 30 degrees. Figure 4 shows that, prior and during the critical roll event, a 2:1 ratio existed between pitch and roll natural frequency. Further, the pitch and roll motions were synchronized. This incident was characterised as a parametric roll resonance event by the ship's owner. The large roll oscillations ceased due to the prompt action of the Master, who altered the heading.

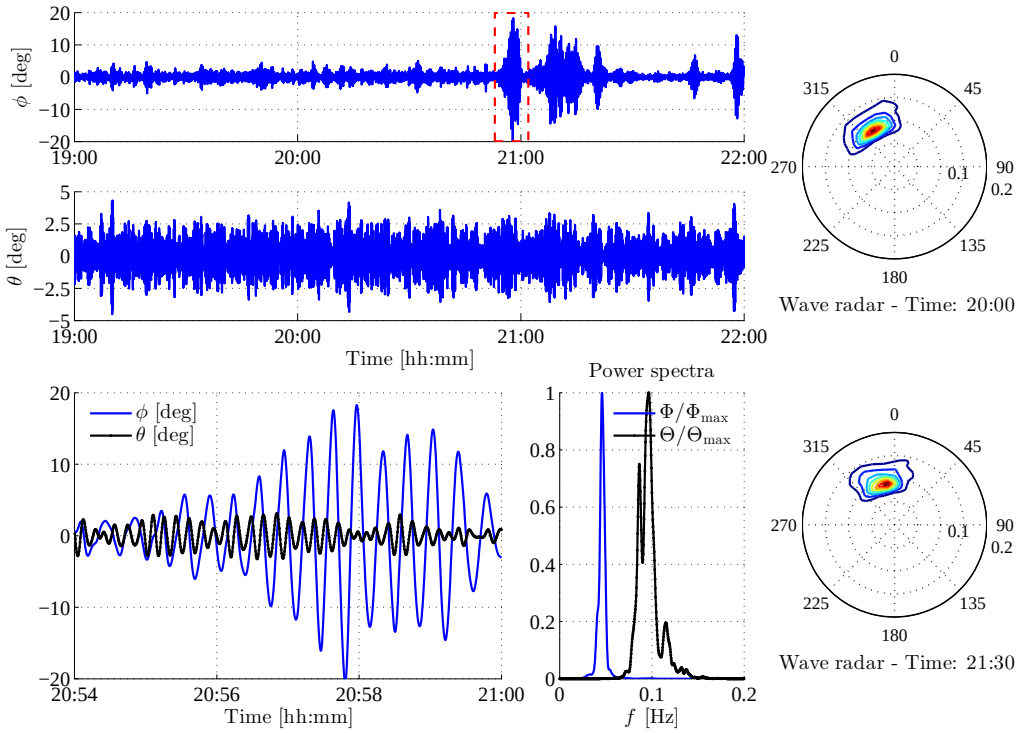

Figure 3: Excerpt of the data set DNV4 from 19:00 to 22:00 hours: occurrences of parametric roll between 21:00 and 22:00 hours is supported by the analysis of the normalized power spectra of pitch and roll, together with the directional wave spectrum and the motions' synchronization.

The second data set (WM2) comprises a 2:1 resonance event in head seas. The relevant time series are seen in Fig. 5. The vessel sailed in head seas and experienced distinct episodes of parametric roll during about four hours, with roll amplitudes up to 20 degrees. Figure 5 illustrates how the 2:1 frequency tuning between pitch and roll persisted during the incident. The Master decided to make a course alteration of about 50 degrees, the result of which was to quickly exit the parametric resonance. Further information on the two incidents are found in (Rosén et al., 2012).

5. Signal-based Detection of Parametric Roll Resonance

An overview of the methods for signal-based detection of parametric roll that were proposed in (Galeazzi et al., 2012b, 2009a,b) and further developed in (Galeazzi et al., 2012a, 2013) is now provided. The empirical methods for the selection of the thresholds for detection based on the statistical analysis of the detectors' outputs will be discussed. Further, the advanced statistical tool for jointly correlated distributions, namely the copula descriptor, will be introduced to analyze the joint probability of false alarms theoretically achievable by the monitoring system through combined hypothesis testing.

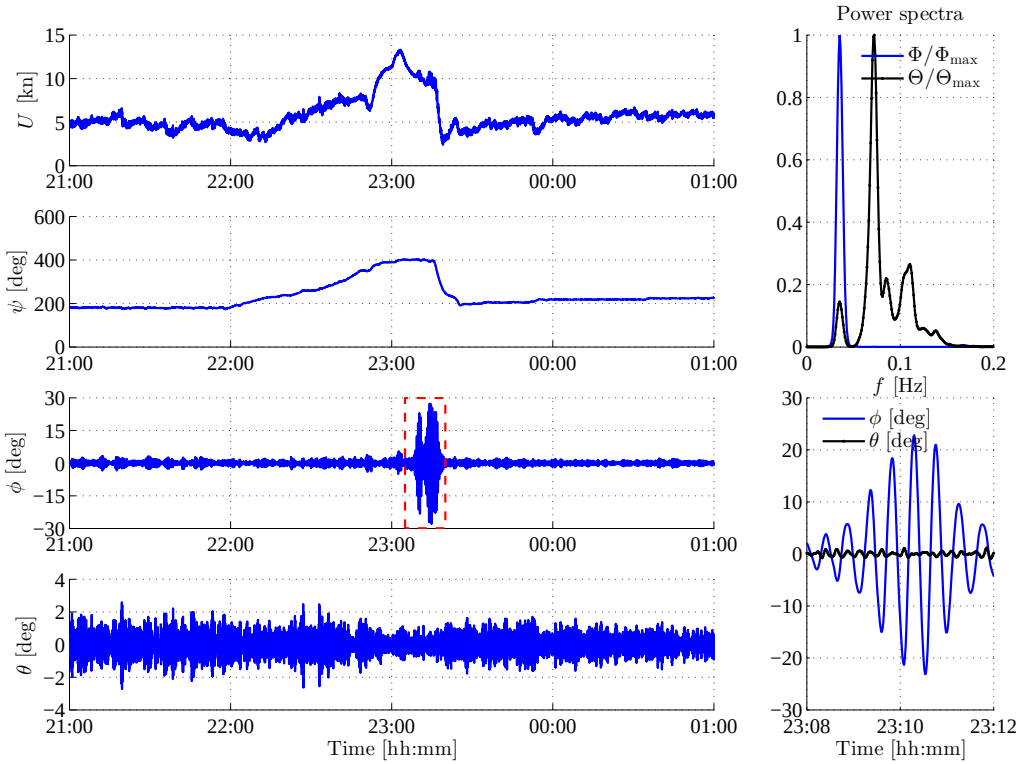

Figure 4: Data set WM1: from top to bottom, ship forward speed, heading angle, roll angle, and pitch angle. A clear parametric roll events takes place right after 23:00 hours, as confirmed by the spectral analysis and synchronization of ship motions.

5.1. Indicators for parametric roll resonance

As discussed in Section 3 the onset and development of parametric roll is due to an indirect energy flow from the wave motion to the roll mode through the nonlinear couplings with the vertical modes, mostly pitch but also heave. This energy transfer is characterized by a sub-harmonic regime, that is the roll oscillations take place at half the pitch frequency, which equals the wave encounter frequency. This physical insight was used in (Galeazzi et al., 2009a) to address the cross-spectrum $P_{\phi^2\theta}(\omega)$ of $\phi^2(t)$ and $\theta(t)$ as a first indicator of the presence of parametric resonance, since $\phi^2(t)$ should reveal an increasing amount of energy near the frequencies where pitch is transferring energy into roll.

Remark. A similar indicator could possibly be derived using heave and roll, since as shown in (Tondl et al., 2000, Chapter 6), (Neves and Rodriguez, 2005), and (Holden et al., 2007a) the vertical displacement is also responsible for the onset and development of parametric roll. However from an operational viewpoint this index may be more cumbersome to compute because a direct measurement of the heave displacement is not readily available onboard, where only accelerations are sensed by the inertial measurement unit (IMU). The pitch angle can instead be directly measured through the installation of an inclinometer or indirectly calculated as a strap-down calculation of the Euler angles based on body rates and acceleration measurements

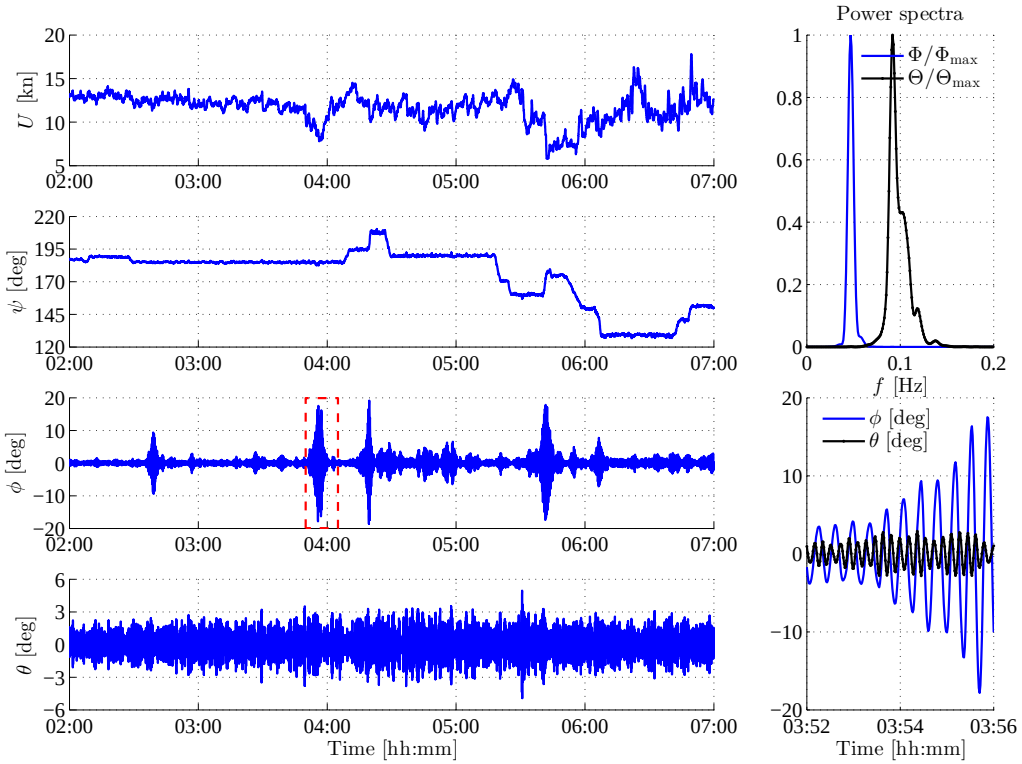

Figure 5: Data set WM2: from top to bottom, ship forward speed, heading angle, roll angle, and pitch angle. During 5 hours the vessel experiences few occurrences of roll resonance with oscillations up to 20 degrees.

provided by the IMU.

The unfolding of parametric roll resonance is also characterized by the non-linear synchronization between motions: as explained in (Døhlie, 2006) a 2:1 synchronization exists between pitch and roll motion, such that every second peak of pitch is in-phase with the peak in roll. An easily available signal that carries information about the phase synchronization of pitch and roll was first proposed in (Galeazzi et al., 2009b),

$$d(t) \triangleq \phi^2(t)\,\theta(t), \qquad t \geq 0. \tag{8}$$

Analysis of motion data, both from model basin and full scale tests (Galeazzi et al., 2013), revealed that the signal $d(t)$ well characterizes the combined pitch and roll motion mode. When the amplitude of $\phi(t)$ abruptly grows, due to parametric resonance, a sequence of negative spikes shows up in $d(t)$. In contrast, when the amplitude of $\phi(t)$ decreases, positive spikes reflect this in $d(t)$. Moreover, when parametric roll is developing, the magnitudes of the negative spikes in $d(t)$ are much larger than those seen when the roll mode is not in the resonant condition.

Since it is the peaks in this signal that indicate synchronization, Galeazzi et al. (2012a) proposed to use the amplitudes of local minima between up-crossings for evaluation,

$$z(k) \triangleq -\min(d(t)), \qquad t \in]T(k-1), T(k)], \tag{9}$$

where $T(k)$ are the time-tags of up-crossings in $d(t)$, and $k \in \mathbb{N}$. This choice greatly reduces the computational burden of the algorithms that carry out the statistical analysis.

5.2. Spectral correlation

The cross-spectrum $\mathcal{P}_{\phi^2\theta}(\omega)$ is exploited to formulate a detection problem in terms of a spectral correlation index, which is defined as

$$\mathcal{S}_{\phi^2\theta} \triangleq \frac{\sigma^2_{\phi^2\theta}}{\sqrt{\sigma^2_{\phi^2}\sigma^2_{\theta}}}, \tag{10}$$

where $\sigma^2_{\phi^2\theta}$ is the power associated to the cross-spectrum within the frequency band of interest $[\omega_1, \omega_2]$, that is

$$\sigma^2_{\phi^2\theta} = \frac{1}{2\pi}\int_{\omega_1}^{\omega_2} \mathcal{P}_{\phi^2\theta}(\omega)\, d\omega, \tag{11}$$

and the normalization factor is introduced to cope with changes in sea state. The signal power of roll squared, $\sigma^2_{\phi^2}$, and pitch, σ^2_{θ}, are calculated over the whole range of frequencies.

The detection problem is written as

$$\begin{aligned} \mathcal{H}_0^S &: \mathcal{S}_{\phi^2\theta} \leq \gamma_S \\ \mathcal{H}_1^S &: \mathcal{S}_{\phi^2\theta} > \gamma_S \end{aligned} \tag{12}$$

where $\mathcal{H}_0^S$ is the case of spectral correlation not being present, and $\mathcal{H}_1^S$ is the case when it is present. The threshold γ_S represents the admissible level of spectral correlation, above which there is a risk of parametric resonance. This *spectral risk* is denoted P_{SR}. The empirical approach to the selection of γ_S is discussed in Section 5.5.

5.3. Phase synchronization

As to the distribution of $z(k)$, a scrutiny showed that a Weibull distribution characterizes $z(k)$ quite well (Galeazzi et al., 2012a). The Weibull distribution has the cumulative distribution function (CDF) and the probability density function (PDF) given by

$$F(z) = 1 - \exp\left(-\left(\frac{z}{\nu}\right)^{\beta}\right), \quad z > 0 \tag{13}$$

$$f(z) = \frac{\beta}{2\nu^{\beta}}\,(z)^{\beta-1} \exp\left(-\left(\frac{z}{\nu}\right)^{\beta}\right), \quad z > 0 \tag{14}$$

where ν and β are scale and shape parameters, respectively.

According to the observations from model test data, a good way to discriminate between resonant and non resonant cases was found to be the change in signal variance. For a Weibull distribution the variance is given by

$$\sigma^2 = \nu^2\left[\Gamma\left(1+\frac{2}{\beta}\right) - \Gamma^2\left(1+\frac{1}{\beta}\right)\right] \tag{15}$$

where $\Gamma(\cdot)$ is the Gamma function. Hence the detection scheme must trail variations in scale and shape parameters.

Assume that the local minima $z(k)$ of the driving signal is a realization of a Weibull random process. Then the distribution of N independent and identically distributed (IID) samples of z has the probability density function

$$f(\mathbf{z};\boldsymbol{\varphi}) = \left(\frac{\beta}{2\nu^{\beta}}\right)^{N} \prod_{k=0}^{N-1} \left[z_k^{\beta-1} \exp\left(-\left(\frac{z_k}{\nu}\right)^{\beta} \right) \right] \tag{16}$$

where $\mathbf{z} = [z(1), z(2), \ldots, z(N)]^{\mathrm{T}}$, and $\boldsymbol{\varphi} = [\nu, \beta]^{\mathrm{T}}$ is the parameter vector of the Weibull PDF. The detection of phase synchronization is therefore formulated as a parameter test,

$$\begin{aligned} \mathcal{H}_0^{\varphi} &: \boldsymbol{\varphi} = \boldsymbol{\varphi}_0 \\ \mathcal{H}_1^{\varphi} &: \boldsymbol{\varphi} \neq \boldsymbol{\varphi}_0 \end{aligned} \tag{17}$$

where $\boldsymbol{\varphi}_0$ characterizes $f(\mathbf{z};\boldsymbol{\varphi})$ in the non-resonant case. By applying the generalized likelihood ratio test (GLRT), the detector decides $\mathcal{H}_1^{\varphi}$ if

$$L_G(\mathbf{z}) = \frac{f\left(\mathbf{z}; \hat{\boldsymbol{\varphi}}, \mathcal{H}_1^{\varphi}\right)}{f\left(\mathbf{z}; \boldsymbol{\varphi}_0, \mathcal{H}_0^{\varphi}\right)} > \gamma \tag{18}$$

where $\hat{\boldsymbol{\varphi}}$ is the maximum likelihood estimate (MLE) of the unknown parameter vector $\boldsymbol{\varphi}$ assuming $\mathcal{H}_1^{\varphi}$ is true. The threshold γ is given by the desired probability of false alarm P_{FA}.

By taking the natural logarithm of both sides of (18) and assuming that the shape parameter is approximately unchanged under both hypothesis – $\beta_1 = \beta_0 = \beta$ – it is possible to show that the test quantity is (see Galeazzi et al. (2012a) for detailed derivations)

$$\mathcal{G}_{\phi^2\theta}(k) = \left(\frac{\hat{\nu}_1(k)}{\nu_0}\right)^{\beta} - 1 - \beta \ln\left(\frac{\hat{\nu}_1(k)}{\nu_0}\right) \tag{19}$$

where

$$\hat{\nu}_1 = \left(\frac{1}{N} \sum_{k=0}^{N-1} z_k^{\hat{\beta}} \right)^{\frac{1}{\hat{\beta}}} \tag{20}$$

$$\frac{1}{\hat{\beta}} = \frac{\sum_{k=0}^{N-1} z_k^{\hat{\beta}} \ln z_k}{\sum_{k=0}^{N-1} z_k^{\hat{\beta}}} - \frac{1}{N} \sum_{k=0}^{N-1} \ln z_k \tag{21}$$

are the maximum likelihood estimates (MLE) of ν_1 and β. The hypothesis $\mathcal{H}_1^{\varphi}$ is then decided if

$$\mathcal{G}_{\phi^2\theta}(k) > \frac{\ln \gamma}{N} = \gamma_G. \tag{22}$$

Remark. The parameter vector $\boldsymbol{\varphi}_0$ characterizing the Weibull distribution under the hypothesis $\mathcal{H}_0^{\varphi}$ is unknown and time-varying due to the non stationarity of the sea state. Hence also $\boldsymbol{\varphi}_0$ is estimated online using the maximum likelihood estimation on a batch of data antecedent to those used for estimating $\boldsymbol{\varphi}$ under the hypothesis $\mathcal{H}_1^{\varphi}$.

Assuming to be at time $t = T$ two phases can be distinguished:

- *Estimation phase:* $\hat{\boldsymbol{\varphi}}_0$ is computed on data logged within the time window $[T - M_{\text{det}} - M_{\text{est}} + 1, T - M_{\text{det}}]$
- *Detection phase:* $\hat{\boldsymbol{\varphi}}$ is computed on data logged within the time window $[T - M_{\text{det}} + 1, T]$

where M_{est} is the estimation window, and M_{det} is the detection window, and $M_{\text{est}} \gg M_{\text{det}}$. A discussion about the choice of M_{est} and M_{det} can be found in (Galeazzi et al., 2013).

When the GLRT-based phase synchronization detector is started an initialization phase is run, where the first M_{est} data samples are used to generate the initial $\hat{\boldsymbol{\varphi}}_0$. During this time the detection is idle since the hypothesis $\mathcal{H}_0^{\varphi}$ is not available yet. This initialization phase is meant to be run when the vessel is leaving the harbour and, hence, absence of parametric resonance can be assumed.

5.4. Combined Hypothesis Testing

The two detectors individually provide reasonable to good performance. The spectral detector gives a probability of being into conditions that could trigger parametric roll, we refer to this as the *spectral risk*, P_{SR}. The phase detector instead should alert only when phase synchronization is present. If this is not the case, a certain false alarm probability P_{FA} will be associated with this detector. With thresholds (γ_S, γ_G) of the two detectors having been chosen from the marginal CDFs for the test quantities, P_{SR} and P_{FA} are determined from[2]

$$P_{SR}(\mathcal{S}|\gamma_S) = 1 - F_S(\gamma_S) \qquad P_{FA}(\mathcal{G}|\gamma_G) = 1 - F_G(\gamma_G) \tag{23}$$

and the marginal distributions F_S and F_G defined as

$$F_S(s) = P\{\mathcal{S} \leq s|\,\mathcal{H}_0\} \qquad F_G(g) = P\{\mathcal{G} \leq g|\,\mathcal{H}_0\} \tag{24}$$

The two detectors can be combined in such a way that an alarm is issued if (and only if) both the detectors threshold values are exceeded. The overall false alarm probability will then be

$$\begin{aligned} P_{FA}(\mathcal{G}, \mathcal{S}) &= P\{\mathcal{G} > \gamma_G \cap \mathcal{S} > \gamma_S|\mathcal{H}_0\} \\ &= P\{\mathcal{G} > \gamma_G|\mathcal{S} > \gamma_S, \mathcal{H}_0\}\, P\{\mathcal{S} > \gamma_S|\,\mathcal{H}_0\}. \end{aligned} \tag{25}$$

It is hence essential to scrutinize the statistical properties of combined hypothesis testing. This requires that a bivariate distribution between the detectors is established. Using the cumulative density functions, it is shown in Appendix A that

$$P_{FA}(\mathcal{G}, \mathcal{S}) = 1 - (F_G(\gamma_G) + F_S(\gamma_S) - F_{GS}(\gamma_G, \gamma_S)), \tag{26}$$

where

$$F_{GS}(g, s) = P\{\mathcal{G} \leq g, \mathcal{S} \leq s\} \tag{27}$$

is the simultaneous CDF.

The joint probability of distributions is conveniently described using the concept of a copula, see e.g (Nelsen, 1999) and (Yan, 2006). A copula describes the joint properties of two variables,

[2] In the sequel $\mathcal{S}_{\phi^2\theta}$ and $\mathcal{G}_{\phi^2\theta}$ are abbreviated to $\mathcal{S}$ and $\mathcal{G}$.

each of which is specified by its marginal distribution. A copula has the advantage over a conventional bivariate description that the marginal distributions can be different and in particular have different weights of their tails, which is important here.

Given two marginal cumulative distributions, $F_S(\mathcal{S})$ and $F_G(\mathcal{G})$, the variables U, V $U = F_G(\mathcal{G}),\ \in [0,1]$ and $V = F_S(\mathcal{S}),\ \in [0,1]$ are uniformly distributed in a unit interval. Then *Sklar's Theorem*, states that the joint distribution of (U, V) is described by the copula,

$$C(u, v) = P\{U \leq u, V \leq v\}, \tag{28}$$

and the bivariate cumulative distribution of $\mathcal{S}$ and $\mathcal{G}$ is then given by

$$F_{GS}(g, s) = C(F_G(g), F_S(s)). \tag{29}$$

The bivariate density function is

$$f_{GS}(g, s) = c(F_G(g), F_S(s))\ f_G(g)\ f_S(s), \tag{30}$$

where c is the density of the copula, and f_G and f_S the PDFs of the marginal distributions. If $\mathcal{G}$ and $\mathcal{S}$ are independent then $c = 1$.

The copula can be estimated from data using a maximum-likelihood approach. A wide range of families of copulas exist with various properties. In this paper the *Frank* copula from the family of *Archimedean Copulas* is used. For the bivariate case the Frank copula is given by

$$C_F(u, v) = -\frac{1}{\xi}\log\left(1 + \frac{(e^{-\xi u} - 1)(e^{-\xi v} - 1)}{e^{-\xi} - 1}\right), \tag{31}$$

where $\xi \in \mathbb{R}\backslash\{0\}$ is the describing parameter.

5.5. Thresholds selection and assessment of false alarm probability

The determination of the thresholds γ_S and γ_G utilized by the monitoring system to alert about the development of a parametric resonance condition are determined empirically by statistical analysis of the outputs generated by the spectral correlation and phase synchronization detectors.

Spectral correlation detector Estimation of the density functions $f(\mathcal{S}; \mathcal{H}_0)$ and $f(\mathcal{S}; \mathcal{H}_1)$ from data is illustrated in Fig. 6. Under the hypothesis $\mathcal{H}_0$ (left plot) the probability chart illustrates that a Gamma distribution better fits $\mathcal{S}_{\phi^2\theta}$ than a Weibull distribution. This is also confirmed by the Kolmogorov-Smirnov goodness-of-fit test with 5% significance level. The Gamma distribution can then be used to assess the spectral risk P_{SR} associated with a given threshold γ_S by calculating the right-tail probability

$$P_{SR}(\mathcal{S}|\gamma_S) = \int_{\{\mathcal{S}:\ \mathcal{S}>\gamma_S\}} f_\gamma(\mathcal{S}; \mathcal{H}_0)\ d\mathcal{S}, \tag{32}$$

where $f_\gamma(\mathcal{S}; \mathcal{H}_0)$ is the Gamma PDF estimated for $\mathcal{S}_{\phi^2\theta}$.

To analyse the hypothesis $\mathcal{H}_1$ the output of the spectral correlation detector for the data sets DNV1 and DNV2 has been considered; in particular values of $\mathcal{S}_{\phi^2\theta}$ larger than 0.1 (truncation point) have been chosen. The probability plot in Fig. 6 is then generated by subtracting the truncation point from the selected data points. A Weibull distribution was used to fit the upper tail ($\mathcal{S}_{\phi^2\theta} \geq 0.01$ corresponding to the true value 0.11), which is the important part to determine the probability of detection.

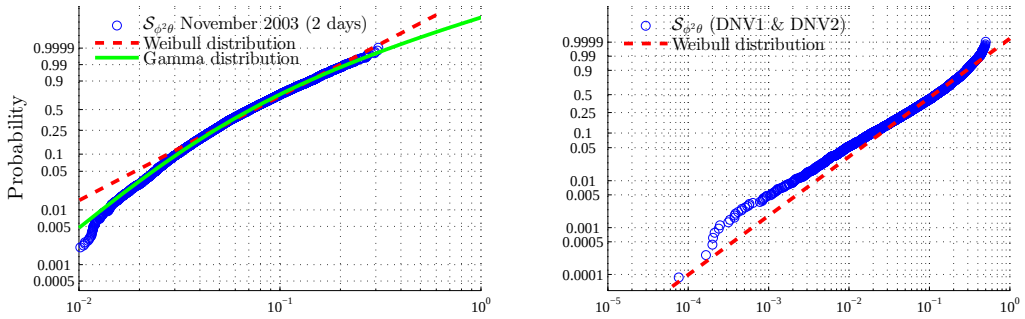

Figure 6: Probability plots of the output of the spectral correlation detector for different DNV-GL data sets. Under the hypothesis $\mathcal{H}_0$ (left plot) the probability chart shows that a Gamma distribution well fits the test statistic of the spectral correlation detector; whereas under the hypothesis $\mathcal{H}_1$ (right plot) a Weibull distribution is used to fit the upper tail.

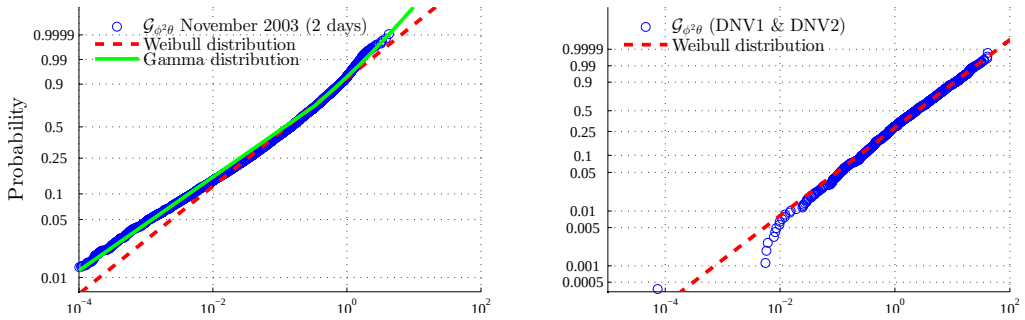

Figure 7: Probability plots of the output of the phase correlation detector for selected DNV-GL data sets. Under the hypothesis $\mathcal{H}_0$ (left plot) the probability chart shows that a Gamma distribution well fits the test statistic of the phase synchronization detector; whereas under the hypothesis $\mathcal{H}_1$ (right plot) a Weibull distribution is the best fit.

Selecting the threshold $\gamma_S = 0.26$ gives a spectral risk $P_{SR} \approx 2 \cdot 10^{-3}$ and a probability of detection $P_D \approx 0.34$.

Phase synchronization detector Figure 7 illustrates the estimated density functions $f(\mathcal{G};\mathcal{H}_0)$ and $f(\mathcal{G};\mathcal{H}_1)$ based on data. Under the hypothesis $\mathcal{H}_0$ (left plot) the probability chart shows that a Gamma distribution represents the output of $\mathcal{G}_{\phi^2\theta}$ better than a Weibull distribution, in particular for what concerns the right-tail of the data that is essential to determine the false alarm probability P_{FA}. The Gamma distribution can then also be used to assess the probability of false alarm of the phase synchronization detector for a given threshold γ_G as

$$P_{FA}(\mathcal{G}|\gamma_G) = \int_{\{\mathcal{G}:\, \mathcal{G}>\gamma_G\}} f_\gamma\left(\mathcal{G};\mathcal{H}_0\right)\, d\mathcal{G}, \tag{33}$$

where $f_\gamma(\mathcal{G};\mathcal{H}_0)$ is the Gamma PDF estimated for $\mathcal{G}_{\phi^2\theta}$.

Under the hypothesis $\mathcal{H}_1$ (right plot) the output of the phase synchronization detector is Weibull distributed. Note that the truncation point here is 1.5, hence the probability plot is built for $\mathcal{G}_{\phi^2\theta} > 1.5$.

Selecting the threshold $\gamma_G = 2.5$ gives a probability of false alarm $P_{FA} \approx 3 \cdot 10^{-3}$, and it guarantees a probability of detection $P_D \approx 0.71$.

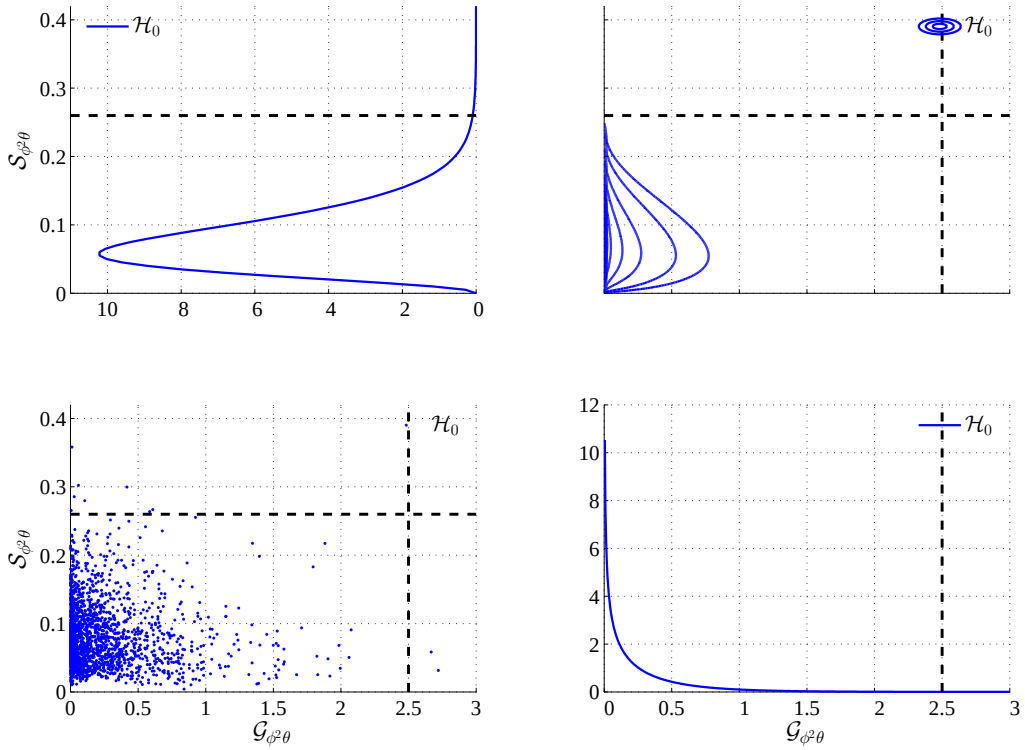

Figure 8: Estimated probability density functions for the two detectors individually and as a bivariate distribution. The blue lines indicate the distribution in $\mathcal{H}_0$. The copula distribution is represented by the contour of its density function. The dashed lines indicate thresholds for detection.

The joint probability is estimated by approximating a *Frank* copula, Eq. 31, to data. Figure 8 shows an example of estimated marginal distributions and corresponding copula estimates using the DNV data set from May on a day without alarms for parametric resonance. The correlation parameter in the estimated copula is used as described in Appendix A in the assessment of false alarm probability as detailed below.

The selected thresholds were used to assess the spectral risk $P_{SR}(\mathcal{S})$ and the probability of false alarm $P_{FA}(\mathcal{G})$ for several data sets differing for type of vessel, type of passage, length of passage, and time of the year. Among all available data sets, those were selected where motions showed spectral correlation in the range 0.05 to 0.15, which is typical for the majority of days recorded.

Figure 9 shows that the chosen thresholds (γ_S, γ_G) determine rather consistent right-tail probabilities across the different data sets, with variations within two order of magnitudes when comparing the two vessels. The Figure also shows the joint probability of false alarm P_{FA} (red bars) calculated according to (26) based on the Frank copula estimated for each data set. It is clear that monitoring system benefits from the combined use of the two detectors, achieving a very low probability of false alarm that in average is around 10^{-6} corresponding to approximately one false alarm every three months.

Remark. The values of the joint probability of false alarm shown in Fig. 9 are based only on

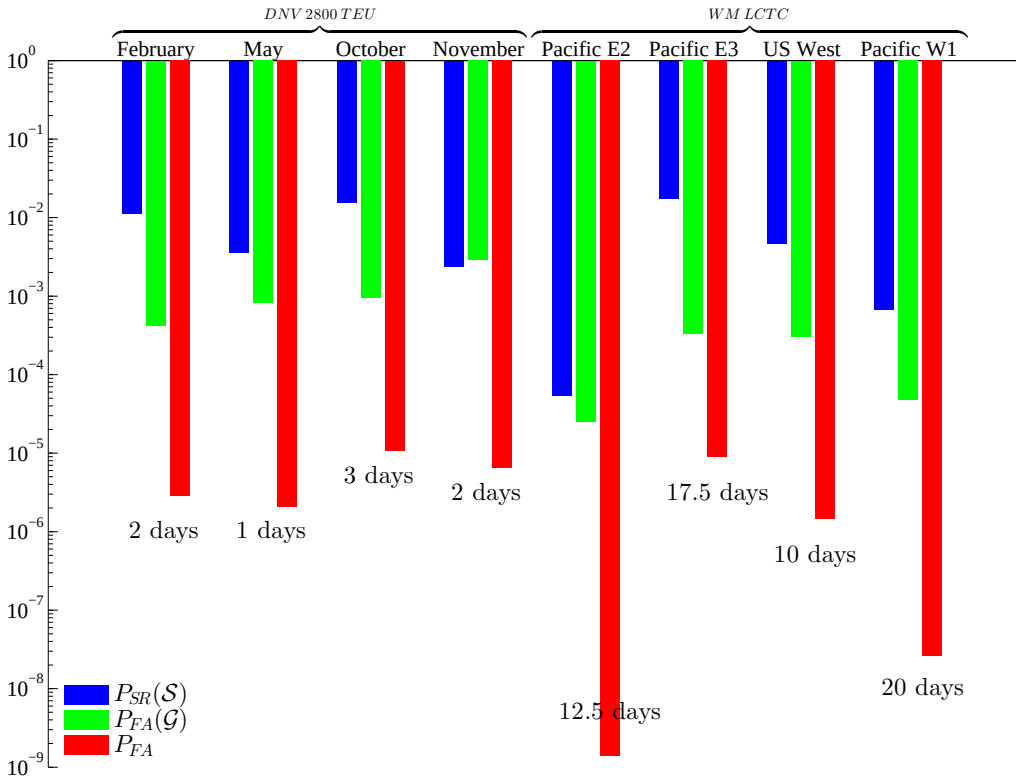

Figure 9: Analysis of the right tail probabilities of the spectral correlation and phase synchronization detectors, and of the joint probability of false alarms. The data sets considered differ for type of vessel, time of the year, and passage.

the statistical properties of the individual detectors combined through the copula estimation. However the monitoring system is implemented with an additional feature that in connection to an alarm evaluates the magnitude of the roll motion. If the roll angle is small then the monitoring system displays only a warning. This further check has been implemented to avoid nuisance on the bridge, where several other systems request the attention of the navigator. Hence the actual value of P_{FA} is lower, and the overall performance is further improved.

5.6. Other detection approaches

Two other approaches for detection of the onset of parametric roll resonance have been reported in literature, where model based methods have been proposed.

Holden et al. (2007b) proposed an observer-based predictor, which estimates the time-varying parameters of a linear second-order oscillatory system driven by white noise. Three different methods were used for estimation, namely Kalman filtering, recursive least squares and particle filtering. Based on the parameter estimates the instantaneous eigenvalues are computed and the algorithm issues a warning when they move outside the unit circle. The method was tested on the same experimental data utilized in (Galeazzi et al., 2009a,b). The observer-based predictor performed very convincingly when tested on data resulting from excitation by narrow band regular waves. However all three methods showed deteriorated performances when tested on data

collected during experiments in irregular waves. The approach was not further developed nor tested on full-scale motion data.

McCue and Bulian (2007) also proposed a model-based approach that uses the finite time Lyapunov exponents (FTLEs) to detect the onset of parametric roll. The roll dynamics in parametric resonance is studied by means of a 1.5 degrees-of-freedom model driven by irregular waves, where the half degree of freedom reflects that heave and pitch are accounted for into the model by means of quasi-static calculation. From the analysis of a large number of simulations it was found that the time-varying behaviour of the FTLEs is not conclusive for the detection of parametric roll as it is instead for the determination of capsizing conditions (McCue and Troesch, 2006). However by observing the behaviour of the sum of the FTLEs "qualitative and potentially quantifiable information is gleaned" (McCue and Bulian, 2007). In particular it is pointed out that a relationship could be established between the behaviour of the sum of the FTLEs and the nonlinear roll damping. In conclusion the behaviour of the FTLEs give some indications of the onset of parametric roll, but these are very much qualitative. The method was not further developed nor tested on model-scale or full-scale motion data.

Some commercial products are also available, where a specific feature for the prediction of the risk of parametric roll is included in the decision support system. Those systems, named first generation warning systems by Døhlie (2006), rely on longer horizon analysis of responses and complex numerical models of the vessel, and provide polar diagrams with risk zones in speed and heading.

Few drawbacks can be outlined when considering designing detection methods based on analytical/numerical models of the vessel. First of all the method is vessel specific and portability of the technology is therefore very much reduced with an implicit increased in cost. Robustness of the method clearly represent an issue, since the specific algorithm depends one way or another on the accuracy of the knowledge of the vessel parameters. The reliability of the method may be linked to the complexity of the used model: accurate predictions of ship motions requires high-fidelity models; this in turn also increases the computation burden. The availability of model parameters still strongly depends on expensive model tests, since the conservatism of the marine industry did not fully open the doors to computational fluid dynamic methods.

These issues have stimulated the signal-based approach proposed in this paper, which attempts to overcome all of them. The presented condition monitoring system relies only on measured signals, roll and pitch, that can be acquired through inexpensive and readily available sensor technology. Moreover, the algorithms run in real-time providing an updated measure of closeness to a parametric resonance condition. Knowledge of the specific vessel is not needed, hence the system is portable and easy to implement.

6. Analysis of Voyage Data

The outcome of the parametric roll monitoring system when tested on the data sets presented in Section 4 is now presented and analysed. Before looking at the single detection cases it is essential to explain what kind of information the following plots display.

As explained in Section 5 the monitoring system integrates the outcomes of the spectral correlation and the phase synchronization detectors in order to decide if a parametric roll resonance event is developing. If both detectors' outputs are above their thresholds then the monitoring system will issue an alarm. This binary output (either alarm or no alarm) is not very adequate from an operational perspective, since it does not allow the navigator to start taking preemptive actions in order to counteract parametric roll and mitigate its possibly devastating effects.

In the light of this the output of the monitoring system has been enhanced with a risk coefficient, which provides a real-time measure of closeness to a parametric roll event by combining the current outputs of the two detectors. The parametric roll risk coefficient is defined as follows.

Definition. Let $\mathcal{S}_{\phi^2\theta}(k)$ and $\mathcal{G}_{\phi^2\theta}(k)$ be the outputs at time k of the spectral correlation and the phase synchronization detectors, respectively. Then the parametric roll risk coefficient at time k is given by

$$\mathcal{R}(k) \triangleq w_1 \mathrm{sat}\left(\frac{\mathcal{S}_{\phi^2\theta}(k)}{\gamma_S}\right) + (1 - w_1)\mathrm{sat}\left(\frac{\mathcal{G}_{\phi^2\theta}(k)}{\gamma_G}\right), \tag{34}$$

where $0 < w_1 < 1$; γ_S and γ_G are the respective thresholds of the two detectors.

Remark. The saturation function sat$(\cdot)$ used in the former definition operates as $\mathrm{sat}\,(x) = x$ if $0 \leq x < 1$ and $\mathrm{sat}\,(x) = 1$ if $x \geq 1$, ensuring $\mathcal{R} \in [0, 1] \subset \mathbb{R}$, with zero corresponding to no risk of parametric roll and one the condition to issue an alarm.

The risk coefficient $\mathcal{R}$ is mapped into a colour coded bar ranging from green (low/no risk of parametric roll), through yellow (moderate risk of parametric roll) to red (high risk of parametric roll). This colour coded information can help in generating a state of alert for the navigator, and eventually enable an immediate reaction if an alarm condition is encountered.

From an operational viewpoint it is also important not to increase the level of nuisance on the bridge where several other decision support systems are integrated. Considering this, the monitoring system has been further enhanced with a check of the roll amplitude, which at last is used to determine whether to issue an alarm. When both detectors are positive the monitoring system evaluates if in the batch of data under analysis the roll amplitude is exponentially growing and if the largest roll peak is greater than an angle, here set to five degrees. If these two additional conditions are concomitantly fulfilled then an alarm is issued, otherwise the alert given by the two detectors is only displayed on the risk bar. This additional check serves as a precautionary measure that allows to avoid giving a full alarm when the amplitude of the roll oscillations is still rather small, while at the same time preserving the needed level of alert due to the actual presence of conditions that could make a parametric roll grow rapidly to large amplitudes. The selection of the roll level serving as a final alarm threshold should be based on firm investigations on officers attitude and it can therefore be tuned on-board to make the best balance between early alerts and avoiding unnecessary alarms on the bridge. It is noted that the (visual) warning level is exclusively based on the statistical risk coefficient (34), while it is solely the audible alarm that can be adjusted to users' needs via the roll level parameter.

The withdrawal of an alarm is managed through return-from-resonance thresholds set at half of the values of γ_S and γ_G (black dashed horizontal lines in the plots of $\mathcal{S}_{\phi^2\theta}$ and $\mathcal{G}_{\phi^2\theta}$ as in Fig. 10). An alarm is withdrawn only if both outputs of the monitoring system are less than the respective return-from-resonance thresholds for one roll period. This approach improve the consistency of the alarm communication policy by avoiding changes of the alarm status based on very short-time variations of the detectors' outputs.

To assess the performance of the monitoring system several quantities have been taken into account, which are defined in the following. Let T_d be the detection time then

- $\phi_d \triangleq \phi(T_d)$ is the value of the roll angle at detection time,
- $\phi^b_{\max} \triangleq \max|\phi(t)|$ for $t \in [T_d - 2T_\phi, T_d[$ is largest peak value in roll achieved within the two roll periods prior to the detection,

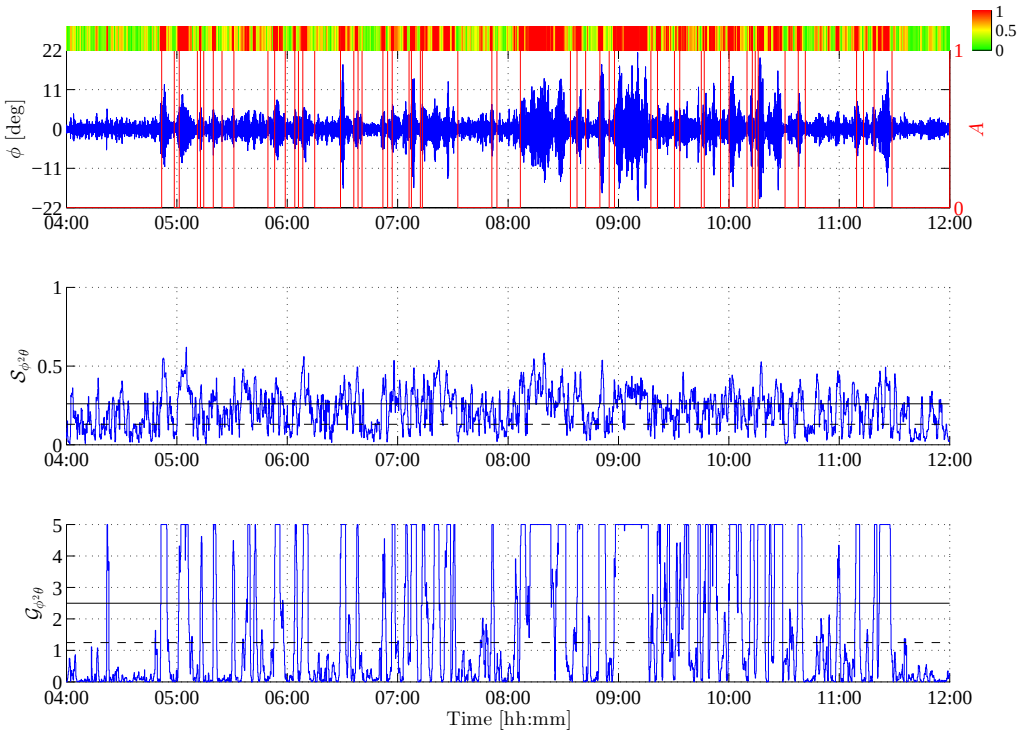

Figure 10: Detection of parametric roll events on DNV3.

- $\phi^w_{\max} \triangleq \max|\phi(t)|$ for $t \in W_d$ is largest peak value in roll achieved within the detection window W_d,
- $T_{\phi_{\max}} \triangleq \arg(\phi^w_{\max}) - T_d$ is the time between the alarm is issued at T_d and $\phi^w_{\max}$ is reached, and it is measured as an integer multiple of the roll period.

6.1. DNV-GL full-scale data set

As pointed out in Section 4.1, the 2800 TEU container vessel was exposed to conditions, which might well lead to parametric roll during four days. This preliminary analysis is completely confirmed by the output of the monitoring system, which issues more than 100 alarms across the four data sets.

Figures 10-11 illustrate the monitoring system's outcome for the two excerpts DNV3 (from 04:00 to 12:00 hours) and DNV4 (from 19:00 to 22:00 hours). In both cases it is interesting to note that the frequency coupling condition is met almost at all times, confirming that the container ship is navigating in conditions very likely to produce parametric resonance, as otherwise already pointed out by the wave radar plots presented in Figs. 2-3. The large number of alarms issued by the monitoring system is simply a consequence of the combination of the sea state, characterized by significant wave height between 5 and 8 meters and peek period between 11 and 13 seconds, with the actions taken by the master of steering more and more the vessel into

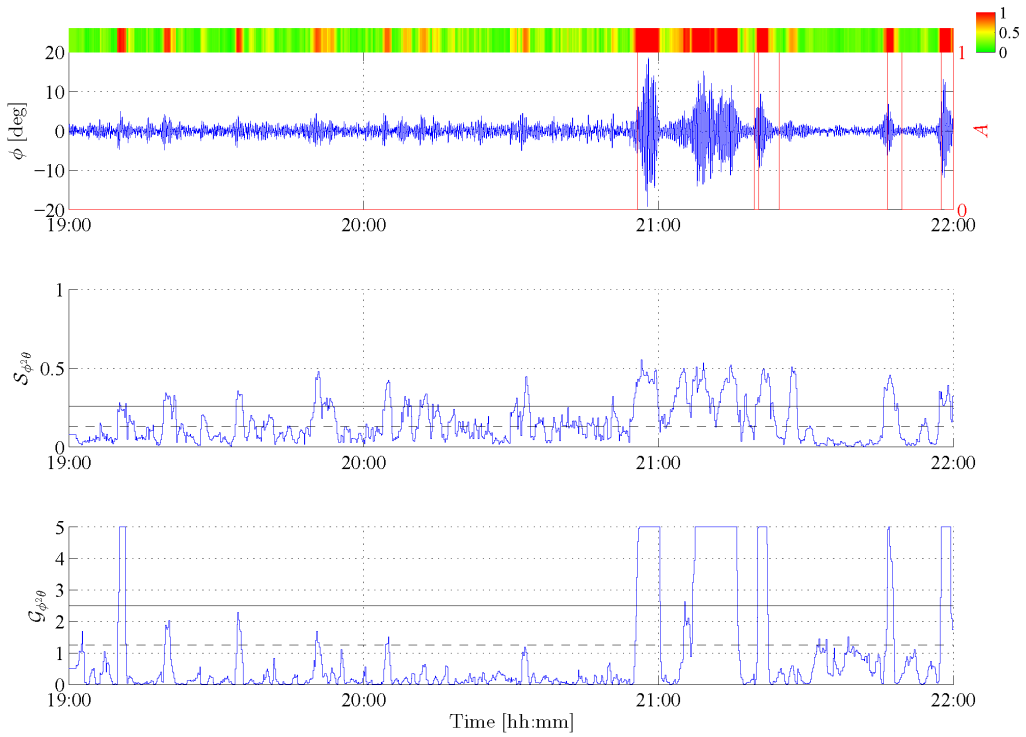

Figure 11: Detection of parametric roll events on DNV4: the monitoring system is giving several warnings of possible parametric resonance occurrence during the two hours prior to the detected events as shown by the risk bar.

the waves and reducing the forward speed in response to the violent roll oscillations, as clearly visible by comparing the top plot of Fig. 2 with the top plot of Fig. 10.

The analysis of the data set DNV4 allows to emphasize how the outcome of the monitor system may support the navigator in having the right level of readiness in facing a parametric roll condition. As shown in the top plot of Fig. 11 the risk bar shows several warnings of possible parametric resonance occurrence during the two hours prior to the actual detected events; hence the monitoring system provides real-time information that the current combination of the sea state with the navigation conditions (forward speed and heading) could lead to the onset and development of parametric roll.

Figure 11 also shows how the alarm withdrawal policy works: at about 21:00 hours the amplitude of the roll motion reduces to less than 5 degrees due to the lost of phase synchronization between roll and pitch as clearly reported by $\mathcal{G}_{\phi^2\theta}$, which sharply falls below its return-from-resonance threshold. However $\mathcal{S}_{\phi^2\theta}$ remains below the return-from-resonance threshold for only half roll period, and then it starts raising again. Therefore the monitoring system keeps the alarm since the frequency coupling condition remains fulfilled, addressing the risk that other parametric roll events may unfold, as it then happens around 21:15 hours.

By comparing the values of the roll angle at detection, ϕ_d, the largest peak right before detection, $\phi^b_{\max}$, and the largest peak within the detection window, $\phi^w_{\max}$ through the histogram in Fig. 12 it is possible to conclude that the monitoring system is indeed capable of providing early

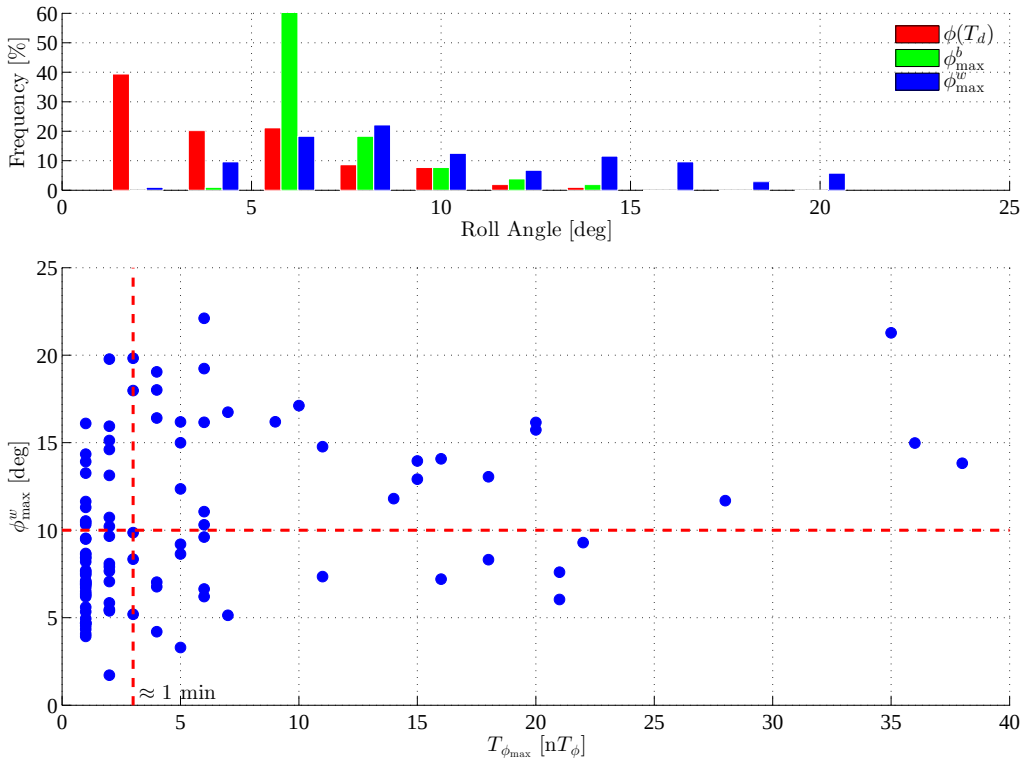

Figure 12: Analysis of the detection outcome for DNV1, DNV2, DNV3, and DNV4. The monitoring system thresholds were set to $\gamma_S = 0.26$ for the spectral correlation detector, $\gamma_G = 2.5$ for the phase synchronization detector, and 5 degrees for the roll amplitude level.

warnings of parametric roll development. In approximately 70% of the issued alarms the largest peak before detection was smaller than 6 degrees ($\phi^b_{\max} \leq 6$ deg), whereas for almost 70% of the cases the largest peak within detection is larger than 8 degrees ($\phi^w_{\max} \geq 8$ deg).

The scatter diagram in Fig. 12 shows the relation between the time $T_{\phi_{\max}}$ and the magnitude of the largest roll displacement within the detection window W_d. From the distribution of the dots in the diagram it is possible to see that vast majority of the detections can be characterized as small and fast resonance events; in fact for approximately 42% of the detections $\phi^w_{\max}$ does not exceed 10 degrees however it is reached in less than 1 minute (approximately 3 roll periods for the considered vessel). Few events of large intensity – $10 < \phi^w_{\max} < 20$ deg – (approximately 17% of the detections) take place shortly after the alarm is given, and they certainly represent challenging situations to counteract. However, the majority of the large parametric roll events – $\phi^w_{\max} > 10$ deg – (approximately 40% of the detections) happen several minutes after the alarm is issued, and this time could be used to take pre-emptive actions in order to possibly avoid or mitigate the effects of large roll accelerations due to the resonance condition.

6.2. Wallenius Marine full-scale data sets

The parametric roll monitoring system performs well also on the data sets WM1 and WM2, as shown in Figs. 13-14.

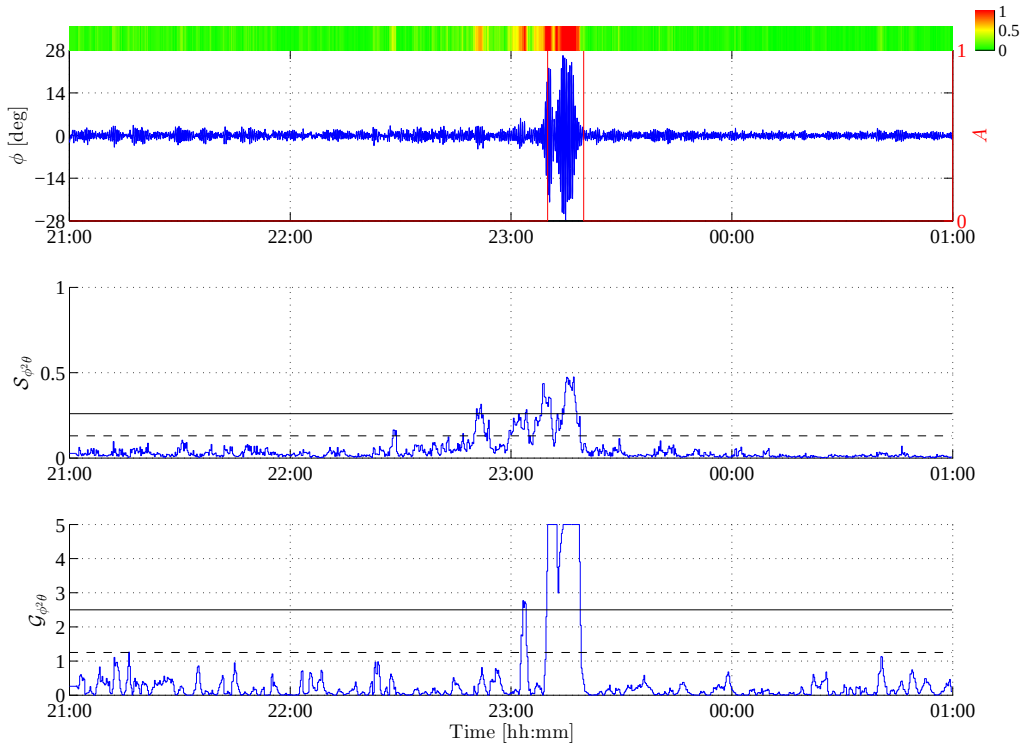

Figure 13: Detection of parametric roll event on WM1.

The outcome of the two detectors confirms the peculiarity of the case depicted in Fig. 13, and the challenge in providing a timely alarm in a situation where parametric roll was certainly not expected: for approximately 2 hours both the spectral correlation and the phase synchronization detectors are well below the respective thresholds. Then, all the sudden when the LCTC has just finished the turnaround manoeuvre (from head sea to following sea) the resonance abruptly kicks in, and induces violent roll oscillations up to 30 degrees. However the monitoring system is not blind to the ongoing changes taking place in the sea-vessel system, and already 20 minutes prior to the alarm the risk bar shows warnings of possible parametric roll (first transition from green to orange approximately about 22:50 hours). The alarm certainly arrives late, when the roll angle has already reached a magnitude of 17 degrees, but it is also certain that the largest roll oscillation peaking at -28 degrees takes place approximately five minutes after the alarm, time that once again could be used to counteract the development of the second and more violent parametric roll event.

The monitoring systems performs extremely well on the data set WM2 where all four major events have been timely detected, as shown in the top plot of Fig. 14. This analysis is also supported by the histograms and scatter diagram in Fig. 15, which clearly show the promptness of the detectors in issuing alarms of parametric roll occurrences. In fact the three resonant events characterized by roll oscillations larger than 15 degrees are detected at least three and a half minutes before the largest roll angle is reached, and that one close to 10 degrees is detected approximately two minutes before the peak value.

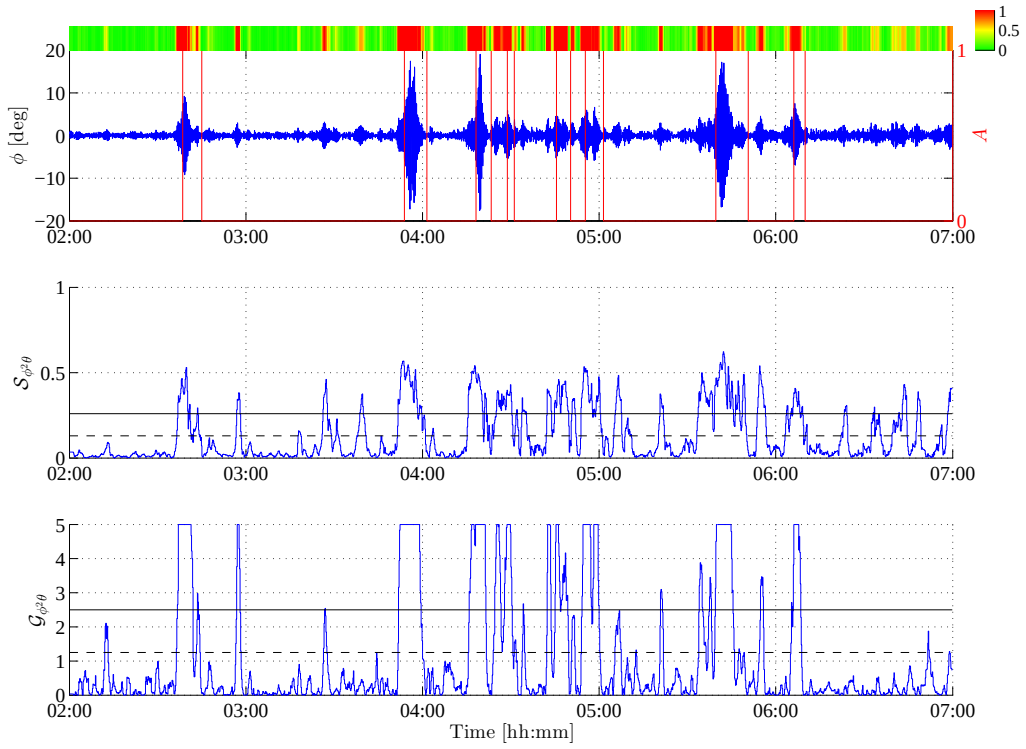

Figure 14: Detection of parametric roll events on WM2.

These four events were already analysed and acknowledged as parametric resonance cases in (Rosén et al., 2012), where a manual assessment was carried out using spectral analysis and graphic comparison or roll and pitch signals in a short time window around the events. However Rosén et al. did not discuss that in between these major events there are smaller parametric roll events with peak amplitudes ranging from 2 to 8 degrees, which instead are precisely detected by the monitoring system.

6.3. Blind test with one-year data from large car carrier

The monitoring algorithms were tested on one year motion data logged on an LCTC from Wallenius Marine. The data logging was made by the Seaware® decision support system that has the ability to transmit 10Hz motion data. No event reports were made by the vessel and no information whatever, other than the logged data, were available to the team who analysed data. Twenty passages for a total of 170 days of navigation have been monitored, and a summary of findings are shown in Fig. 16 where for each passage information about voyage length, number of parametric roll alarms issued (number atop each bar), and total time the spectral correlation condition was fulfilled is provided.

No particular events had been reported from the vessel, but the monitoring algorithms found several incidents over the year where parametric resonance conditions were present but roll amplitude did not develop to critical magnitudes. In particular one record, on an Eastwards Pacific passage, see Fig. 17, shows a parametric roll event where the amplitude of roll grows rapidly

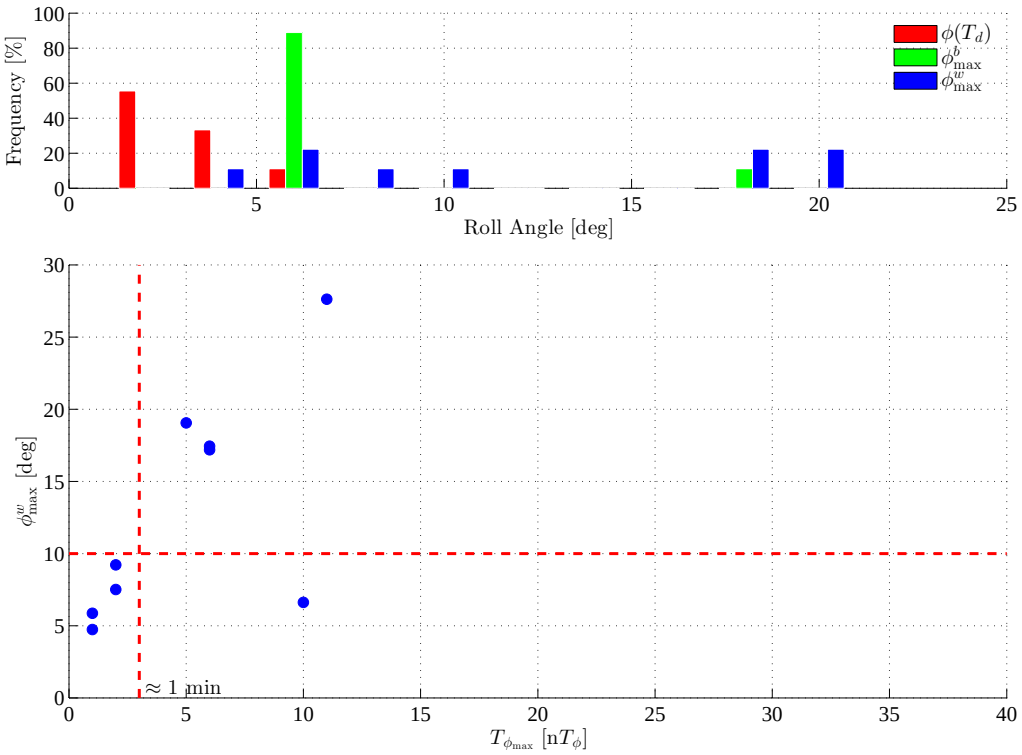

Figure 15: Analysis of the detection outcome for WM1, and WM2. The monitoring system thresholds were set to $\gamma_S = 0.26$ for the spectral correlation detector, $\gamma_G = 2.5$ for the phase synchronization detector, and 5 degrees for the roll amplitude level.

from 4 to 9 degrees of amplitude. The incident did not develop to serious amplitudes as the maximum roll angle stayed within 10 deg. The motion records show that spectral conditions were present for a 2:1 resonance during several days of the passage, and sea conditions apparently developed such that phase synchronisation appeared several times around the main event. Inspecting the risk bar in Fig. 17 shows that the warning level (yellow to orange colour) develops to high risk level (dark orange) well ahead of the onset of resonance (red colour in risk bar and alert flag changing from 0 to 1) where an alert is issued.

The main event was spotted independently of this study by Wallenius Marine by means of a post processing analysis software that search for events of high or rapidly growing roll. The events with smaller amplitudes were not noticed by this post processing software.

Detection of several short and low amplitude events during the year shows the efficacy of the monitoring algorithms presented here, and the occurrence of a number of small-amplitude events could be expected for vessels that are susceptible to parametric roll. Studies on probability of parametric roll in random seas Jensen (2012) related the time invariant peak distribution of roll to be exponentially decreasing with an exponent being the square of the inverse of significant wave height.

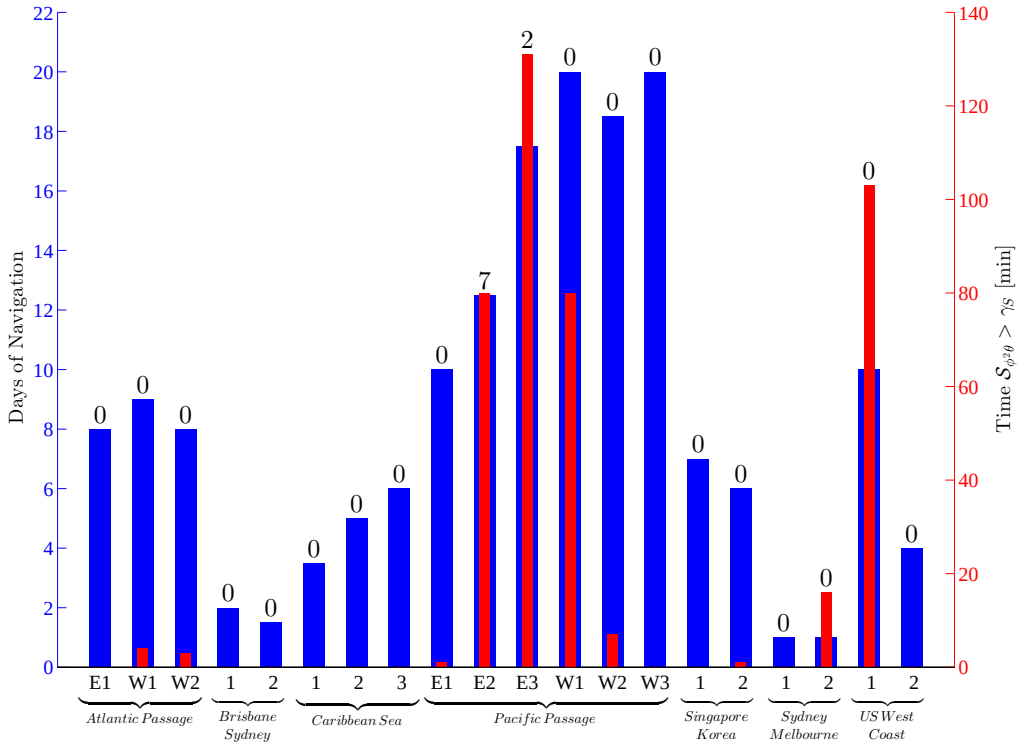

Figure 16: Results of one year monitoring of LCTC. The numbers atop each bar is number of detected events. The red inserts show the time elapsed within which the spectral correlation index exceeded the threshold γ_S. The letters "E" and "W" indicate Eastbound and Westbound, respectively.

7. Perspectives

Many ship owners and operators are nowadays aware of the risk associated with parametric roll, and, consequently, they develop strategies to manage this phenomenon. Mitigating risk from parametric roll at Wallenius Marine currently includes a chain of activities (Huss, 2014)

- Design optimization based on extensive numerical simulations to ascertain ships' hull forms that are sufficiently robust for their intended service
- Education of all officers on stability variations in waves in general, on the specific characteristics and service experience of different generations of vessels and on decision support systems on-board
- Use of decision support systems including:
  - route planning and optimization based on forecasted weather conditions including, among other criteria, assessment of the risk for parametric roll along the route
  - real-time assessment of the sea conditions (Ovegård et al., 2012), with warnings and advice on possible actions for avoiding high risk situations

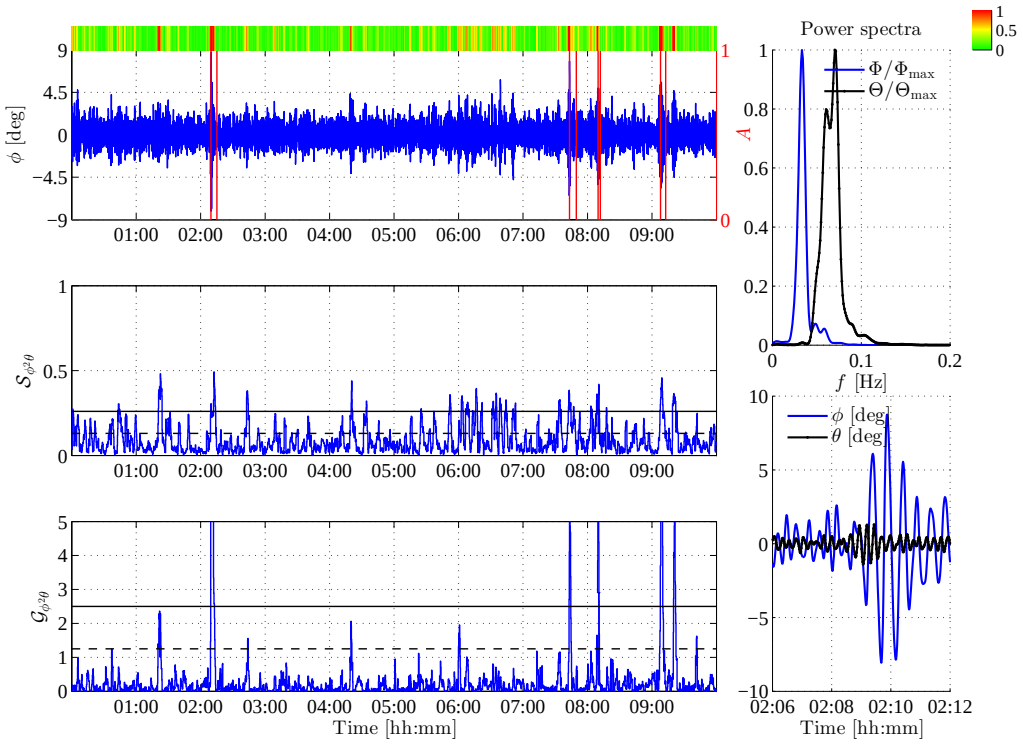

Figure 17: Detection of few parametric roll events onboard a LCTC during a eastward crossing of the Pacific ocean. The spectral analysis and the time domain comparison of roll and pitch confirm the presence of conditions for the unfolding of parametric roll resonance.

  - real-time monitoring of motions, as presented in this paper, to warn about onset of parametric resonance

- Regular procedures for following up and analysing all events that may contribute to increased knowledge and awareness, including perhaps automated analysis using monitoring algorithms as described in this paper.

With these actions Wallenius aims at having very few events with parametric roll in the future and none with a severe outcome. The statistical analysis of motion data from the past three years indicates that parametric roll of any significance is already at a very low rate, and larger events are reported only about once per five ship years for the latest generations of ships.

The IMO working group on intact stability is currently considering similar schemes, and in the near future it may propose them as mandatory for vessels that are vulnerable to large stability variations in waves. This may be in force worldwide within the next few years.

Development of active systems that could directly interfere with the growth of large roll motions is currently ongoing. These systems would be extensions to rudder-roll damping concepts (Perez and Blanke, 2012), and they aim at integrating early detection algorithms with compensating rudder actions. Wallenius is currently participating in developing and testing such systems (Söder et al., 2013), that would form the last link in the chain of actions for managing the risk of

parametric roll.

8. Conclusions

Through access to extensive data sets, sampled at 5 Hz and above, this paper scrutinized full-scale motion data during long periods of normal passage and during several days where roll resonance was present or conditions were very close to resonance. A monitoring methodology was tested that is based on indicators for frequency and phase synchronization in the 2:1 resonance mode. The presence of both conditions simultaneously, was confirmed to be a sure indicator for the presence of parametric resonance. Using statistical methods, the two indicators were used for detecting the presence of one or both of the conditions. Modelling of the bivariate distribution of the test statistics for the two indicators was done using copula methods, and it was shown how false alarm and detection probabilities were derived from the parameters of the copula and from those of the marginal distributions that describe the test statistics of each of the indicators. A salient feature of the monitoring methodology was that it is based on measurements from inexpensive inertial measurement units.

It was found that a learning approach, where thresholds are automatically calculated from motion data when resonance is not present, created the required robustness of the monitoring scheme and made the detection methods insensitive to changes in weather conditions.

Analysis of the performance of the parametric roll monitoring method, referred to as PAROLL, considered time to largest roll amplitude after an alert was issued, maximum roll angle immediately before an alert, and the maximal roll angle during resonance conditions. These data showed that the officers would normally have sufficient time to react from the main alert but also that warnings were available in all cases that conditions were present for parametric resonance to develop if irregular seas happened to come into tune with the resonance conditions for a short period of time.

From long time investigations of motion data from a large car carrier and a feeder size container vessel it is possible to conclude that parametric resonance is by far more common than reported, but it is rarely developing into serious magnitudes. With the monitoring principles tested in this paper, early detection is available such that remedial actions can be taken well before parametric roll develops to severe magnitudes.

Few interesting elements need to be addressed in the future work: as the use of bivariate statistical analysis has shown beneficial in order to evaluate the real life probability of false alarm of the combined detection algorithms, the same statistical tools could be used to theoretically assess the joint probability of detection and hence formally prove that the fusion of the output of the two detectors into the condition monitoring system enhances the overall detection performance. Integration of additional signals such as roll and pitch rates or angular accelerations could be shown beneficial in order to further reduce the detection time. Inclusion of adaptive thresholds could further increase robustness towards changing sea states. Last, from a scientific and operational point of view it would be extremely interesting to investigate vessel's motions after an alarm is raised and the navigator has taken countermeasures to evaluate if and when exiting a parametric roll resonance condition is possible.

Appendix A. False alarm probability for bivariate distribution

This appendix derives the false alarm probability for a bivariate distribution. With classification area for $\mathcal{H}_1$ being Ω_1 the false alarm rate is, by definition,

$$P_{FA} = \int_{\Omega_1} f(\mathcal{G}, \mathcal{S}|\mathcal{H}_0)\, d\mathcal{S}\, d\mathcal{G} = \int_{\gamma_G}^{\infty} \int_{\gamma_S}^{\infty} f(\mathcal{G}, \mathcal{S}|\mathcal{H}_0)\, d\mathcal{S}\, d\mathcal{G} \tag{A.1}$$

Using in (A.1) that

$$\int_{\gamma_S}^{\infty} f(\mathcal{G}, \mathcal{S}|\mathcal{H}_0)\, d\mathcal{S} = \int_{0}^{\infty} f(\mathcal{G}, \mathcal{S}|\mathcal{H}_0)\, d\mathcal{S} - \int_{0}^{\gamma_S} f(\mathcal{G}, \mathcal{S}|\mathcal{H}_0)\, d\mathcal{S},$$

gives

$$\begin{aligned} P_{FA} &= \int_0^{\infty} \left[\int_0^{\infty} f(\mathcal{G}, \mathcal{S}|\mathcal{H}_0)\, d\mathcal{S} - \int_0^{\gamma_S} f(\mathcal{G}, \mathcal{S}|\mathcal{H}_0)\, d\mathcal{S} \right] d\mathcal{G} \\ &\quad - \int_0^{\gamma_G} \left[\int_0^{\infty} f(\mathcal{G}, \mathcal{S}|\mathcal{H}_0)\, d\mathcal{S} - \int_0^{\gamma_S} f(\mathcal{G}, \mathcal{S}|\mathcal{H}_0)\, d\mathcal{S} \right] d\mathcal{G} \\ &= 1 - \int_0^{\gamma_S} f(\mathcal{S}|\mathcal{H}_0)\, d\mathcal{S} - \int_0^{\gamma_G} f(\mathcal{G}|\mathcal{H}_0)\, d\mathcal{G} \\ &\quad + \int_0^{\gamma_G} \int_0^{\gamma_S} f(\mathcal{G}, \mathcal{S}|\mathcal{H}_0)\, d\mathcal{S}\, d\mathcal{G}\,. \end{aligned} \tag{A.2}$$

Therefore the false alarm probability for a bivariate distribution is given by

$$\begin{aligned} P_{FA} &= 1 - (F_S(\gamma_S) + F_G(\gamma_G) - F_{GS}(\gamma_G, \gamma_S)) \\ &= P_{SR}(\mathcal{S}|\gamma_S) + P_{FA}(\mathcal{G}|\gamma_G) - P_{FA}(\mathcal{G}, \mathcal{S}|\gamma_G, \gamma_S) \end{aligned} \tag{A.3}$$

References

Boonstra, H.A., Blok, J.B., van Daalen, E.B., 2006. Towards a risk-based approach of intact stability of ships in a seaway. Harbin Gongcheng Daxue Xuebao/Journal of Harbin Engineering University 27, 50–58.

Bulian, G., Francescutto, A., Umeda, N., Hashimoto, H., 2008. Qualitative and quantitative characteristics of parametric ship rolling in random waves in the light of physical model experiments. Ocean Engineering 35, 1661–1675.

Carmel, S.M., 2006. Study of parametric rolling event on a panamax container vessel. Journal of the Transportation Research Board 1963, 56–63.

Døhlie, K.A., 2006. Parametric rolling – a problem solved? DNV Container Ship Update 1, 12–15.

France, W.N., Levadou, M., Treakle, T.W., Paulling, J.R., Michel, R.K., Moore, C., 2001. An investigation of head-sea parametric rolling and its influence on container lashing systems, in: SNAME Annual Meeting.

Galeazzi, R., Blanke, M., Poulsen, N.K., 2009a. Detection of parametric roll resonance on ships from indication of nonlinear energy flow, in: Proc. 7th IFAC Symposium on Fault Detection, Supervision and Safety of Technical Processes.

Galeazzi, R., Blanke, M., Poulsen, N.K., 2009b. Parametric roll resonance detection using phase correlation and log-likelihood testing techniques, in: Proc. of the 8th IFAC Int. Conference on Manoeuvring and Control of Marine Craft, pp. 316–321.

Galeazzi, R., Blanke, M., Poulsen, N.K., 2012a. Detection of parametric roll for ships, in: Fossen, T.I., Nijmeijer, H. (Eds.), Parametric Resonance in Dynamical Systems. Springer. chapter 2, pp. 17–45.

Galeazzi, R., Blanke, M., Poulsen, N.K., 2012b. Prediction of resonant oscillation, EP2419804.

Galeazzi, R., Blanke, M., Poulsen, N.K., 2013. Early detection of parametric roll resonance on container ships. IEEE Transactions on Control Systems Technology 21 (2), 489–503.

Grimshaw, R., 1993. Nonlinear Ordinary Differential Equations. CRC Press.

Hashimoto, H., Umeda, N., 2004. Nonlinear analysis of parametric rolling in longitudinal and quartering seas with realistic modelling of roll-restoring moment. Journal of Marine Science and Technology 9, 117–126.

Holden, C., Galeazzi, R., Rodríguez, C., Perez, T., Fossen, T.I., Blanke, M., Neves, M.A.S., 2007a. Nonlinear container ship model for the study of parametric roll resonance. Modeling, Identification and Control 28, 87–113.

Holden, C., Perez, T., Fossen, T.I., 2007b. Frequency-motivated observer design for the prediction of parametric roll resonance, in: Proc. of the 7th IFAC Conference on Control Applications in Marine Systems.

Huss, M., 2014. What is parametric roll? The Swedish Club Triton 1, 22–24.

Jensen, J.J., 2007. Effcient estimation of extreme non-linear roll motions using the first-order reliability method (FORM). Journal of Marine Science and Technology 12, 191–202.

Jensen, J.J., 2012. Probability of parametric roll in random seaways, in: Fossen, T.I., Nijmeijer, H. (Eds.), Parametric Resonance in Dynamical Systems. Springer. chapter 5, pp. 91–107.

Koning, J., 2010. Lashing@Sea - Executive summary. Technical Report. MARIN.

Krüger, S., Hatecke, H., Billerbeck, H., Bruns, A., Kluwe, F., 2013. Investigation of the 2nd generation of intact stability criteria for ships vulnerable to parametric rolling in following seas, in: Proc. of the Int. Conference on Offshore Mechanics and Arctic Engineering - OMAE.

McCue, L.S., Bulian, G., 2007. A numerical feasibility study of a parametric roll advance warning system. Journal of Offshore Mechanics and Arctic Engineering 129, 165–175.

McCue, L.S., Troesch, A.W., 2006. A combined numerical-empirical method to calculate finite time Lyapunov exponents from experimental time series with application to vessel capsizing. Ocean Engineering 33(13), 1796 – 1813.

Nelsen, R.B., 1999. An Introduction to Copulas. Springer. 2^{nd} edition.

Neves, M.A.S., Rodriguez, C.A., 2005. A coupled third order model of roll parametric resonance, in: Soares, C.G., Garbatov, Y., Fonseca, N. (Eds.), Maritime Transportation and Exploitation of Ocean and Coastal Resources, Taylor & Francis. pp. 243–253.

Neves, M.A.S., Rodriguez, C.A., 2006. On unstable ship motions resulting from strong non-linear coupling. Ocean Engineering 33, 1853–1883.

Ovegård, E., Rosén, A., Palmquist, M., Huss, M., 2012. Operational guidance with respect to pure loss of stability and parametric rolling, in: Proc. 11^{th} Int. Conf. on the Stability of Ships and Ocean Vehicles.

Perez, T., Blanke, M., 2012. Ship roll motion control. Annual Reviews in Control 36, 129–147.

Rosén, A., Huss, M., Palmquist, M., 2012. Experience from parametric rolling of ships, in: Fossen, T.I., Nijmeijer, H. (Eds.), Parametric Resonance in Dynamical Systems. Springer. chapter 8, pp. 147–166.

Söder, C.J., Rosén, C., Ovegård, E., Kuttenkeuler, Huss, M., 2013. Parametric roll mitigation using rudder control. Journal of Marine Science and Technology 18(3), 395–403.

Tondl, A., Ruijgrok, T., Verhulst, F., Nabergoj, R., 2000. Autoparametric Resonance in Mechanical Systems. Cambridge University Press.

Yan, J., 2006. Multivariate modeling with copulas and engineering applications, in: Pham, H. (Ed.), Springer Handbook of Engineering Statistics. Springer. chapter 51, pp. 973 – 990.